9-10-2010

Effect of air on vibration of structures

Tong Xia

EFFECT OF AIR ON VIBRATION OF STRUCTURES

BY

TONG XIA

THESIS

Submitted in Partial Fulfillment of the
Requirements for the Degree of

MASTER OF SCIENCE
CIVIL ENGINEERING

The University of New Mexico
Albuquerque, New Mexico

July 2010

This thesis is dedicated to my parents.

ACKNOWLEDGEMENTS

I would like to thank the United States Department of Energy (award no. DE-FG52-08NA28782), the National Science Foundation (award no. IIS-0813747), and Sandia National Laboratories who supported this work.

I would like to thank my advisor Dr. Walter Gerstle who offered me this valued opportunity and help during my studies. Thank you for your kindness and patience, and all your knowledge that was shared with me.

I would like to thank Dr. Steven Griffin who provided valuable suggestions for my research.

I would like to thank Dr. Majeed Hayat and Dr. Timothy Ross for their support and guidance.

Also, I would like to thank Mr. Luke Graham who was always happy to offer help with the software LABVIEW.

EFFECT OF AIR ON VIBRATION OF STRUCTURES

BY

TONG XIA

ABSTRACT OF THESIS

Submitted in Partial Fulfillment of the
Requirements for the Degree of

MASTER OF SCIENCE
CIVIL ENGINEERING

The University of New Mexico
Albuquerque, New Mexico

July 2010

EFFECT OF AIR ON VIBRATION OF STRUCTURES

TONG XIA

B.E., Bridge Engineering, Chang An University, 2007

M.S., Civil Engineering, University of New Mexico, 2010

ABSTRACT

This research primarily studies the effect of air on vibration of structures. Theoretical solutions based on various physics are derived and compared with experimental results to determine how air modifies the vibrational behavior of structures. This work may help in determining the characteristics of structural vibrations – from acoustic behavior to earthquake response - in practical buildings.

The work consists of several primary components: derivation of theories that predict the effect of air on structural vibrations and vice-versa, design of experiments, and determination of the importance of air in structural vibrations and the applicability of different physics under various vibrational frequencies.

Two types of physics - acoustic theory and fluid dynamics theory - are applied to derive solutions for damping ratios of air. Experiments such as an unbaffled plate experiment, a pendulum experiment and a baffled plate experiment are designed and conducted to observe the damping effect of air. Experimental results illustrate the applicability of the theories. Finite element analysis is performed to provide a

computational basis with which to compare the observed vibrational frequencies.

The main question in this research is whether air has a great effect on structural vibrations. The results show that air has a damping effect on vibrating buildings that can be important under certain conditions. The results also reveal that when calculating the damping effects due to air, different physics should be applied under different vibrational conditions. A dimensionless factor is derived to determine under which regimes acoustic theory is applicable, and under which regimes fluid dynamics theory is applicable.

Table of Contents

4. Acoustic Damping of Spheres

5. Energy Dissipation: Fluid Dynamics Theory

6. A Baffled Piston: Rayleigh Integral Solution

7. Unbaffled Plate Experiment

8. Pendulum Experiment

9. Baffled Piston Experiment

10. Analysis and Discussion

11. Conclusion

CHAPTER 1.

INTRODUCTION

1.1 General

Acoustic-structure interaction problems include sound generated from vibrating structures and the effects of sound on adjacent structures and buildings. The applications of these problems include noise control, military detection, and industrial design. In this field, acoustic theory is commonly used.

On the other hand, the discipline of *fluid-structure interaction* models the behavior of structures which are surrounded by a fluid medium, such as air or water. The applications of this field include ship design, aeronautical design and so on. Fluid dynamics theory is commonly used to solve fluid-structure interaction problems.

In practice, most structures are exposed to both sound and air. As a result the rigorous analysis of structures requires that structural dynamics, acoustic theory and fluid dynamics theory be applied simultaneously. According to Ross [2004], a medium such as air which is a fluid capable of transmitting sound is called an acoustic fluid, and this field is called *acoustic fluid-structure interaction*.

The study and application of acoustic fluid-structure interaction problems is limited due to its extreme complexity. It is possible that under specific acoustic frequencies, a harmonic frequency of a structure could be excited, leading to large-scale vibration and even failure of the structure. An example is a lady who sings

at a certain pitch, causing a wine glass to break. Meanwhile, the air inside and outside of the structure could affect the vibrational modes and natural frequencies of the structure. During earthquakes, the air surrounding a building could have a damping effect upon the vibration; on the other hand, it could also intensify the vibration under certain vibrational frequencies. Structural safety concerns lead us to inquire whether the presence of air will affect vibrational behaviors, possibly leading to structural failure. As a result, it is interesting to study acoustic fluid-structure interaction problems to better understand the effects of air and sound upon structural vibrations. This thesis presents a study of acoustic fluid-structure interaction problems by comparing theoretical solutions based on different types of physics to designed experimental results.

1.2 Background

The Electrical & Computer Engineering Department and the Civil Engineering Department at the University of New Mexico are collaborating on research to use synthetic aperture radar to monitor activities within buildings. The main target of this research project is to determine the characteristics of the machinery inside a building whose vibrations are being monitored. As part of this collaborative research project, this thesis follows and extends the research conducted previously by Lee [2006] and Ortega [2008].

Lee [2006] determined how air affects the response of a given structure theoretically and experimentally. He demonstrated finite element software's capability to calculate a structure's natural frequencies. Ortega [2008] presented a

detailed study of a fluid-structure interaction problem in both an analytical and an experimental manner. Solutions for gas-solid interaction problems were developed. It was also discovered by using finite element software that the presence of air within an enclosed structure introduces extra vibrational modes beyond those found in the structure without enclosed air.

The discoveries of Ortega [2008] are also confirmed by the current research. By using the finite element software, ANSYS, two separate structures are modeled. One structure representing an airless room in vacuum is compared with another one with enclosed air. The natural frequencies of the rooms are calculated and vibrational mode shapes are generated. It is confirmed that the presence of air can affect the modes of a given structure. Air also introduces extra vibrational modes in addition to the vibrational modes in the air-absent model.

An experimental approach is also developed to demonstrate the applicability of the 1D gas-solid interaction solution derived by Ortega [2008]. The solution correctly predicts the natural frequencies of the system.

In this thesis, analytical and experimental approaches are developed in an effort to better understand the characteristics of acoustic fluid-structure interaction. Two types of physics are employed: acoustic theory and fluid dynamics theory. Note that both acoustic theory and fluid dynamics theory are extensive fields. However in this thesis when mentioning acoustic theory, it refers to small-deformation, irrotational flow, linear vibration of a fluid; on the other hand, when mentioning fluid dynamics theory, it refers to more-or-less steady fluid flow past a solid body. Fluid dynamics

theory includes irrotational flows and turbulence, but not the high-frequency vibrations usually called “acoustics”.

1.3 Motivation

This thesis is motivated by the desire to answer the following questions:

(1) Under what conditions does air affect the vibration of a building structure?

(2) How important is the effect of air on a vibrating building structure? Should we consider air in analyzing buildings?

(3) Under what conditions does a building structure’s vibration cause sound and related acoustic effects in air?

(4) What type of physics should be used in determining structural damping due to air resistance?

(5) When is acoustic theory appropriate, and when is fluid dynamics theory appropriate?

(6) Can we develop simple formulas that predict the damping effect of air on buildings?

The objectives and scope of this thesis are presented next.

1.4 Objectives and Scope

Chapter 2 describes literature related to this thesis. These published works include studies of acoustic-structure interaction and fluid-structure interaction. This literature review shows that researchers have mostly attempted to solve specific problems. No experimental approaches appear to have focused on the applicability of different physical regimes of behavior.

To study the damping effect of air based on acoustic theory, we need to understand acoustic theory first. Chapter 3 presents analytical solutions for the acoustic energy radiated from pulsating and oscillating spheres.

Chapter 4 relates the acoustic theory in chapter 3 to the analytical solutions for the damping ratio of a vibrating structure. An expression for the damping effect of air based on acoustic theory is obtained.

To study the damping effect of air based on fluid dynamics theory, chapter 5 presents the analysis of drag and lift forces due to fluid flow. The work done by these forces is related to the energy dissipated from a vibrating structure. The derivation of the equivalent damping ratio of air based on dissipated fluid energy is presented.

For comparison purposes, the effect of air upon a baffled vibrating piston is next studied in chapter 6, which presents the derivation of the solution called the Rayleigh Integral, which calculates the farfield pressure due to a vibrating baffled piston.

Chapter 7 presents a vibrating unbaffled plate experiment to verify the applicability of the equation derived in chapter 3. Acceleration data is acquired and the damping ratio is calculated based on test data.

Chapter 8 presents a pendulum experiment to verify the applicability of the equation derived in chapter 5. Displacement data is acquired and the damping ratio is calculated based on test data.

Chapter 9 presents a baffled vibrating elastic plate experiment to verify the applicability of the equation derived in chapter 6. Pressure and acceleration data is acquired. The result is compared with the Rayleigh Integral solution.

Chapter 10 analyzes the experimental results. A dimensionless variable is proposed to determine the applicability of acoustic theory and fluid dynamics theory.

Chapter 11 presents the conclusions and recommends future research directions.

The next chapter describes the literature relevant to this research.

CHAPTER 2.

LITERATURE REVIEW

2.1 General

Research in both the field of fluid-structure interaction and the field of acoustic-structure interaction has been extensive. In the acoustic-structure interaction field, it is assumed that a sound wave propagates through a fluid by interacting with particles (molecules or atoms). The particle motions are assumed to be very small compared to the wave length. Various theoretical approaches such as classical mechanical solutions and finite element solutions have been developed to describe the behaviors of both the fluid and the structure.

On the other hand, fluid-structure interaction uses classical fluid dynamics theory to determine the behavior of the fluid. Within the scope of this thesis, fluid dynamics theory assumes constant speed fluid flow in which the particle motions are large, compared to acoustic theory. Lift and drag coefficients are used to predict the interaction between the fluid and the adjacent structure.

As stated before, structures are exposed to both sound and air. It is then reasonable to study the case when both acoustic and fluid dynamics theories are applied simultaneously, which is referred to as acoustic fluid-structure interaction. However, literature in this field is very limited. This thesis is a continuation study of a research project studying a structure's mechanical vibration due to machinery;

therefore previous research conducted by three former graduate students from the University of New Mexico is presented next.

Mareddy [2006] presented an experiment measuring vibration data gathered from an existing utility building at the University of New Mexico to see if types of machinery use can be determined from vibration data. Acceleration data was acquired at various locations on the roof of the building. A Matlab code called VIBVIS was developed for interpreting and visualizing the acquired data. A modal analysis of the building was performed using finite element software SAP2000 to compare with the experimentally measured vibrations. Results showed that it is possible to determine whether there is machinery being operated within a building by measuring roof accelerations. However it remains difficult to determine which type of machine is being used.

An experiment was developed by Lee [2006] studying the interaction of air with a single degree of freedom structure. The vibration data of the structure was collected under both maximum and minimum air resistance cases. Damping ratios were calculated for both cases when the structure is built with various stiffnesses. Results showed a clear difference between the maximum and the minimum air resistance cases. A finite element model was also developed in SAP 2000, and modal analysis was performed. Results showed good agreement between the tested natural frequencies and the computer generated natural frequencies.

As a continuation of this research, Ortega [2008] presented a study on an essential dynamic gas-solid interaction problem. Both an analytical solution and a

finite element discrete solution for the problem were developed. A one-dimensional gas-solid interaction experiment was designed to verify the solutions. The finite element software ANSYS was also applied to simulate the complicated two-dimensional gas-solid interaction. Results showed that the presence of air adjacent to a vibrating structure introduces extra modes.

To continue with this project, this thesis is devoted to study acoustic fluid-structure interaction. A review of related research is presented next.

2.2 Papers from Research Journals

Kozien and Wiciak [2005] studied the acoustic radiation emitted from a specific vibrating folded plate. The acoustic pressure level at a certain control point was simulated using finite element software. The results showed that finite element software facilitates the analysis of the pressure field at a given point, but a complete description of mechanical and acoustical aspects of the problem is computationally expensive. No experimental approach was reported. The analysis is restricted to the high-frequency range. No low-frequency vibrations were considered.

Osaka [2007] presented an experiment with a rectangular aluminum plate vibrating under harmonic excitations. Plastic coatings were attached to the plate to provide internal damping effects. By changing the coatings, different damping effects were produced. Both experimental and finite element analyse were performed to study the influence of internal damping on vibration and acoustic radiation characteristics. The results showed that the internal damping from coatings does not affect the natural frequencies of the system; however it introduces both the changing of mode shapes

and the amplitude of displacement. The researcher ignores the effect of the surrounding air.

Decultot, Lietard and Chati [2008] presented an experiment measuring the energy radiated from an immersed vibrating plate in water. Vibrational modes were identified and comparisons were made between finite element software results and experimental results. Under a sinusoidal driving force, the radiated pressure was measured. Good agreement was found between the experimental radiated pressure peaks and the theoretical results. A finite element model also calculated the expected modes and natural frequencies. It was demonstrated that it is possible to measure the acoustic radiation using a hydrophone.

Hasheminejad and Azarpeyvand [2003] studied the acoustic radiation emitted from an oscillating sphere within a fluid. Numerical results showed the effects of vibrational frequency and mode of vibration on the farfield pressures. They also showed the relationship between the properties of the fluid and the farfield acoustic pressure amplitude. The theoretical solution and computer-based simulations showed that the farfield acoustic pressure is frequency-sensitive. However no experiments were developed.

Research in acoustic fluid-structure interaction tends to be very specific and practical because any variable change could lead to a basic change in applicability of theories. Thus, to understand the fundamentals of the problem, the basic theories are studied next.

2.3 Textbooks

Structures and buildings often vibrate in two modes which can be thought of as either a radially pulsating sphere or a transversely oscillating sphere. Due to the simplification provided by spherical coordinates, the spherical model is broadly used to simplify the derivation of acoustic power radiated from vibrating structures.

Pierce [1989] provided a solution for the acoustic power radiated from a radially pulsating sphere. A velocity potential was employed to express the fluid velocity and pressure of a spherically symmetric wave. A transient solution for the acoustic field radiated by a sphere was derived. The time-averaged power radiated from the pulsating sphere was derived from the solution when the sphere is pulsating at a constant frequency. The time average of the acoustic power radiated from a transversely oscillating sphere was also derived.

Blackstock [2000] reached the expression for the energy radiated from a pulsating sphere using an alternative path by using the concept of impedance. The mechanical power radiated from an oscillating body was first related to acoustic density, which could be expressed in terms of impedance. The impedance was then expressed in either Cartesian coordinates or polar coordinates in terms of fluid pressure and velocity. Finally, the power radiated from the pulsating sphere was expressed in terms of fluid properties and vibrational properties.

Blackstock [2000] also derived the solution for farfield pressure amplitude of a vibrating target. This solution was first derived by Lord Rayleigh [1842-1919]. A model of a baffled circular piston was used to derive the pressure distribution in the

farfield beyond the distance called the Rayleigh Distance. Details of this derivation are discussed in chapter 6.

The fluid dynamics theory used in this thesis is from Roberson and Crowe [1975], who derived the expression for the drag force and lift force caused by fluid flows. The drag coefficient is used to predict the fluid-induced forces acting upon structures with various shapes. More details of this derivation are discussed in chapter 5.

The next chapter presents the derivation of the three-dimensional acoustic governing differential equation. The expressions for the acoustic energy radiated from a pulsating sphere and an oscillating sphere are also presented.

CHAPTER 3.

ACOUSTIC THEORY AND ENERGY RADIATED FROM PULSATING AND OSCILLATING SPHERES

To study the effect of air on the vibration of structures, we need to build mathematical models. A radially pulsating sphere and a transversely oscillating sphere are the two simple analytical models we choose to apply to study structural vibrations. The vibrations and their resulting sound radiations are described using spherical coordinates for convenience. Therefore, the main purpose of this chapter is to derive expressions for the sound power radiated from a pulsating sphere and an oscillating sphere. In chapter 4, the expressions will be used to approximate damping behavior of a vibrating structure.

To derive expressions for the acoustic radiation from pulsating and oscillating spheres, let us start with the derivation of the three-dimensional acoustic governing differential equation, which is commonly called the wave equation.

3.1 Basic Theory of Acoustics

Blackstock [2000] presents a detailed derivation of the three-dimensional wave equation in spherical coordinates. This process is summarized in this section.

3.1.1 Conservation of Mass

Consider the flow of fluid through a differential volume, $dV = dxdydz$, fixed in space, shown in Fig. 3.1.

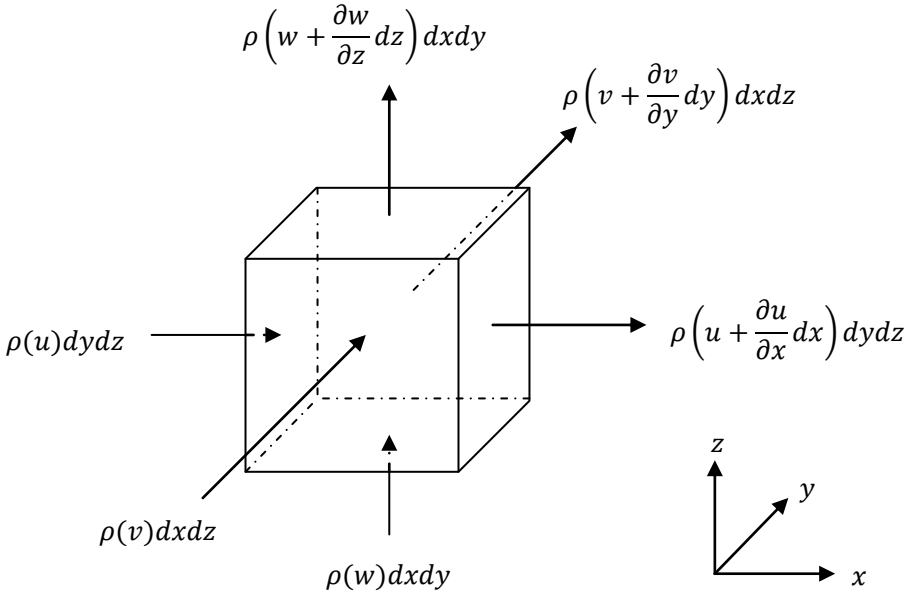

Fig. 3.1: Flow of Mass through a Fixed Volume Element

In Fig. 3.1, u, v and w are the velocity components of the flow and ρ is the density of the fluid.

According to Antoine Lavoisier [1711-1765], who first outlined the law of conservation of mass, the mass of the isolated system remains unchanged as a result of processes acting upon the system. Therefore, for the fixed block in Fig. 3.1, it is required that the time rate of increase of mass inside the volume dV is equal to the net mass inflow through surface of dV. In mathematical form,

$$\frac{\partial}{\partial t}(\rho dxdydz) = \rho dydz\left(u-\left(u+\frac{\partial u}{\partial x}dx\right)\right) + \rho dzdx\left(v-\left(v+\frac{\partial v}{\partial y}dy\right)\right) + \rho dxdy\left(w-\left(w+\frac{\partial w}{\partial z}dz\right)\right). \qquad (Eq.\,3.1)$$

After simplification, Eq. 3.1 is written as:

$$\frac{\partial \rho}{\partial t} + \frac{\partial (\rho u)}{\partial x} + \frac{\partial (\rho v)}{\partial y} + \frac{\partial (\rho w)}{\partial z} = 0 \ , \qquad (Eq. 3.2)$$

or

$$\frac{\partial \rho}{\partial t} + \boldsymbol{\nabla} \cdot (\rho \mathbf{u}) = 0 \ , \qquad (Eq. 3.3)$$

where $\mathbf{u}$ is the fluid velocity vector and $\mathbf{u} = \mathbf{i}u + \mathbf{j}v + \mathbf{k}w$. $\boldsymbol{\nabla}$ is the divergence operator, which is defined as:

$$\boldsymbol{\nabla} \cdot \mathbf{u} = \frac{\partial u}{\partial x} + \frac{\partial v}{\partial y} + \frac{\partial w}{\partial z}$$

Eq. 3.3 is the equation of conservation of mass.

3.1.2 Conservation of Momentum

Consider the spatially-fixed reference volume, V, shown in Fig. 3.2. According to Newton's second law, the rate of change of the momentum of the volume is proportional to the resultant forces acting on the volume. Here the resultant forces are momentum inflow through the surface area S and the sum of the exterior forces.

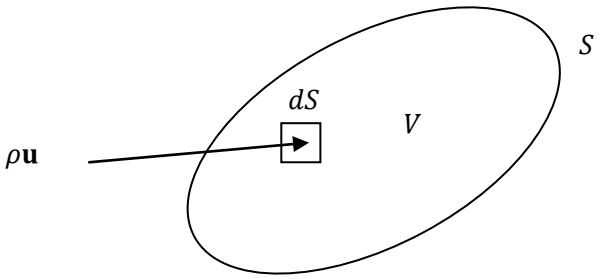

Fig. 3.2: Momentum Flow through an Arbitrary Volume, V

Assume the fluid is inviscid (no shear stresses). The exterior forces consist of two parts, the surface force $\boldsymbol{F_s}$ and body force $\boldsymbol{B}$. Here the surface force is considered as pressure due to the adjacent air. The body force is considered as the force due to gravity. Thus,

$$Exteror\ forces = \boldsymbol{B} + \boldsymbol{F_s} = \int_V \boldsymbol{B}\rho dV - \int_S P d\boldsymbol{S} \ . \qquad (Eq. 3.4)$$

The minus sign of the surface force indicates that the pressure, P, is inward pointing normal to the surface S.

The quantity $(\rho\mathbf{u})[\mathbf{u}\cdot(-d\boldsymbol{S})]$ is the momentum per unit time carried by the inflowing fluid into the volume V through the infinitessimal element with area, dS. The total momentum inflow into V is obtained by integrating over the surface, S. Thus, the mathematical form of conservation of momentum is expressed as:

$$\frac{\partial}{\partial t}\int_V \rho\mathbf{u}dV = \int_V \boldsymbol{B}\rho dV - \int_S P d\boldsymbol{S} - \int_S (\rho\mathbf{u})(\mathbf{u}\cdot d\boldsymbol{S}) \ . \qquad (Eq.3.5)$$

According to Gauss's divergence theorem, the surface integrals can be converted to volume integrals:

$$\int_S P d\boldsymbol{S} = \int_V \boldsymbol{\nabla} P dV \ ;$$

$$\int_S (\rho\mathbf{u})(\mathbf{u}\cdot d\boldsymbol{S}) = \int_V \boldsymbol{\nabla}[(\rho\mathbf{u})\cdot\mathbf{u}]dV \ .$$

Substituting the converted integrals above into Eq. 3.5, the momentum equation can be rewritten as:

$$\frac{\partial}{\partial t}\int_V \rho\mathbf{u}dV = \int_V \boldsymbol{B}\rho dV - \int_V \boldsymbol{\nabla} P dV - \int_V \boldsymbol{\nabla}[(\rho\mathbf{u})\cdot\mathbf{u}]dV \ . \qquad (Eq.3.6)$$

Bringing the time derivative operation inside the integral and rearranging, we obtain

$$\int_V (\rho\mathbf{u})_t dV - \int_V \rho\boldsymbol{B}dV + \int_V \boldsymbol{\nabla} P dV + \int_V \boldsymbol{\nabla}[(\rho\mathbf{u})\cdot\mathbf{u}]dV = 0 \ .$$

Collecting terms:

$$\int_V \{(\rho\mathbf{u})_t + \boldsymbol{\nabla}[(\rho\mathbf{u})\cdot\mathbf{u}] + \boldsymbol{\nabla} P - \rho\boldsymbol{B}\}dV = 0 \ . \qquad (Eq.3.7)$$

Assuming the volume V is arbitrary, then

$$(\rho\mathbf{u})_t + \boldsymbol{\nabla}[(\rho\mathbf{u}) \cdot \mathbf{u}] + \boldsymbol{\nabla}P = \rho\boldsymbol{B} \ . \qquad (Eq.3.8)$$

Ignoring the force due to gravity, the body force on the right side vanishes. Expanding the first two terms, we obtain:

$$\rho_t\mathbf{u} + \rho\mathbf{u}_t + [\boldsymbol{\nabla} \cdot (\rho\mathbf{u})]\mathbf{u} + (\boldsymbol{\nabla} \cdot \mathbf{u})(\rho\mathbf{u}) + \boldsymbol{\nabla}P = 0 \, .$$

According to the equation of conservation of mass (Eq. 3.3), the first and the third term of the above equation vanish. We obtain the three-dimensional momentum equation as

$$\rho[\mathbf{u}_t + (\boldsymbol{\nabla} \cdot \mathbf{u})\mathbf{u}] + \boldsymbol{\nabla}P = 0 \ . \qquad (Eq.3.9)$$

The material derivative of a vector is defined as

$$\frac{D\mathbf{u}}{Dt} = \frac{\partial\mathbf{u}}{\partial t} + \mathbf{u}(\boldsymbol{\nabla} \cdot \mathbf{u}) \ . \qquad (Eq.3.10)$$

Thus Eq. 3.9 can be written as:

$$\rho\frac{D\mathbf{u}}{Dt} + \boldsymbol{\nabla}P = 0 \ . \qquad (Eq.3.11)$$

Eq. 3.11 is the vector form of the equation of conservation of momentum.

3.2 Three-Dimensional Wave Equation

Assuming $\rho \cong \rho_0$, which is the steady state of density, the linear form of Eq. 3.3 is:

$$\delta\rho_t + \rho_0\boldsymbol{\nabla} \cdot \mathbf{u} = 0 \ , \qquad (Eq.3.12)$$

where the function $\delta\rho$ is defined as the excess density:

$$\delta\rho \equiv \rho - \rho_0 \ . \qquad (Eq.3.13)$$

According to Pierce [1989], the static properties of a fluid, such as static density, ρ_0 and static pressure, p_0, refer to the density and pressure of the fluid in which

acoustic perturbation is absent.

The linear from of Eq. 3.11 is:

$$\rho_0 \mathbf{u}_t + \boldsymbol{\nabla} P = 0 \ . \qquad (Eq. 3.14)$$

Introducing the velocity potential, ϕ, which is defined by

$$\mathbf{u} = \boldsymbol{\nabla}\phi \ , \qquad (Eq. 3.15)$$

and substituting Eq. 3.15 into Eq. 3.14, we obtain:

$$\rho_0 \boldsymbol{\nabla}\phi_t + \boldsymbol{\nabla} P = 0 \ . \qquad (Eq. 3.16)$$

Integrating Eq. 3.16, we obtain

$$P = -\rho_0 \phi_t + C \ , \qquad (Eq. 3.17)$$

where C is a constant and can be neglected. The isentropic equation of state in an acoustic field is given as:

$$P = c_0 \delta\rho \ . \qquad (Eq. 3.18)$$

where $\delta\rho \equiv \rho - \rho_0$, and c_0 is the speed of sound in a static fluid. Combining the equation of continuity (Eq. 3.3), the momentum equation (Eq. 3.1), the velocity potential (Eq. 3.15) and the equation of state (Eq. 3.18), we obtain:

$$\nabla^2 \phi - \frac{1}{{c_0}^2} \phi_{tt} = 0 \qquad (Eq. 3.19)$$

Solving Eq. 3.19 gives the velocity potential ϕ, thus the pressure and particle velocity can be found from Eq. 3.15 and Eq. 3.17. The velocity potential is a convenient way to describe an acoustic field in terms of a single scalar function from which other quantities can be derived.

3.2.1 Solutions for One-Dimensional Waves

The three one-dimensional forms of Eq. 3.19 are:

Plane waves:

$$\phi_{xx} - \frac{1}{c_0^2}\phi_{tt} = 0 \ . \qquad (Eq.3.20)$$

Cylindrical waves:

$$\phi_{rr} + \frac{1}{r}\phi_r - \frac{1}{c_0^2}\phi_{tt} = 0 \ . \qquad (Eq.3.21)$$

Spherical waves:

$$\phi_{rr} + \frac{2}{r}\phi_r - \frac{1}{c_0^2}\phi_{tt} = 0 \ . \qquad (Eq.3.22)$$

For a spherical wave, the general wave form is obtained from Eq. 22 as follows.

Multiplying both sides of Eq. 3.22 by r :

$$2\phi_r + r\phi_{rr} - \frac{1}{{c_0}^2}(r\phi)_{tt} = 0 \ ,$$

$$\phi_r + \phi_r + r\phi_{rr} - \frac{1}{{c_0}^2}(r\phi)_{tt} = 0 \ ,$$

$$(\phi + r\phi_r)_r - \frac{1}{{c_0}^2}(r\phi)_{tt} = 0 \ ,$$

$$\nabla^2(r\phi) - \frac{1}{{c_0}^2}(r\phi)_{tt} = 0 \ . \qquad (Eq.3.23)$$

The general solution of the plane wave equation $c^2\nabla^2 u - u_{tt} = 0$ is in the form:

$$u = f(x - ct) + g(x + ct) \ . \qquad (Eq.3.24)$$

Since Eq. 3.23 has the same form as the plane wave equation, their solutions should have the same form. Thus the general solution for Eq. 3.23 is

$$r\phi = f(r - c_0 t) + g(r + c_0 t) \ , \qquad (Eq.3.25)$$

or

$$\phi = \frac{f(r - c_0 t)}{r} + \frac{g(r + c_0 t)}{r} \ , \qquad (Eq.3.26)$$

where the first term represents an outgoing wave while the second term represents an incoming wave. Another form of solution is also available. In certain cases this form

of solution will simplify calculations.

$$\phi = \frac{F(t - r/c_0)}{r} + \frac{G(t + r/c_0)}{r} \quad . \qquad (Eq. 3.27)$$

This form of the solution will be used in the next section.

3.2.2 Solutions for Waves from Pulsating Sphere

To determine the wave motion in the fluid field in which there is a pulsating sphere, assume the radius of the sphere is r_0, and the vibrational frequency of the sphere is ω. The boundary conditions are:

(1) The velocity potential, ϕ varies sinusoidally in a form of $\phi = A \sin \omega t$ at the surface of the sphere, $r = r_0$.

(2) When $r > r_0$, that is, when it is in the fluid field, reflections and absorptions from the farfield are neglected. Thus there are no incoming waves and the second term of Eq. 3.27 vanishes.

From boundary condition (1) and Eq. 3.27, we obtain

$$\phi = A \sin \omega t = \frac{F(t - r_0/c_0)}{r_0} \quad . \qquad (Eq. 3.28)$$

Now $F(t)$ is solved by replacing $t - r/c_0$ as t:

$$F(t) = r_0 A \sin \omega \left(t + \frac{r_0}{c_0} \right) \quad . \qquad (Eq. 3.29)$$

The final solution is in the form:

$$\phi = \frac{F(t - r/c_0)}{r} = \frac{r_0 A}{r} \sin \omega \left(t - \frac{r}{c_0} + \frac{r_0}{c_0} \right) \quad . \qquad (Eq. 3.30)$$

Define wave number, $k = \omega/c_0 = 2\pi/\lambda$, where λ is the wave length, Eq. 3.30 can be finally written as

$$\phi = \frac{A r_0}{r} \sin[\omega t - k(r - r_0)] \quad . \qquad (Eq. 3.31)$$

This is the velocity potential solution for waves from a pulsating sphere.

3.3 Radiation from a Pulsating Sphere

The fluid velocity vector **u** has been defined in Section 3.1.1. In spherical coordinates, from Eq. 3.31, the velocity vector is written as:

$$\mathbf{u} = \phi_r = -\frac{Ar_0}{r^2}\sin[\omega t - k(r - r_0)] - \frac{kAr_0}{r}\cos[\omega t - k(r - r_0)] \ . \qquad (Eq.3.32)$$

The pressure is related to ϕ_r through Eq. 3.17. Thus, in spherical coordinates:

$$P = -\rho_0\phi_t = -\frac{\omega\rho_0 Ar_0}{r}\cos[\omega t - k(r - r_0)] \ . \qquad (Eq.3.33)$$

When $r = r_0$, the velocity at the surface of the sphere is

$$\begin{aligned}\mathbf{u}(\mathrm{r}_0) &= -\frac{Ar_0}{{r_0}^2}\sin[\omega t - k(r_0 - r_0)] - \frac{kAr_0}{r_0}\cos[\omega t - k(r_0 - r_0)] \\ &= -\frac{A}{r_0}\sin(\omega t) - kA\cos(\omega t) \\ &= -\frac{A}{r_0}[\sin(\omega t) + kr_0\cos(\omega t)] \ ; \qquad (Eq.3.34)\end{aligned}$$

and when $r = r_0$, the pressure at the surface of the sphere is

$$\begin{aligned}P(r_0) &= -\frac{\omega\rho_0 Ar_0}{r_0}\cos[\omega t - k(r_0 - r_0)] \\ &= -\omega\rho_0 A\cos(\omega t) \ . \qquad (Eq.3.35)\end{aligned}$$

Now consider the work done by the sphere's surface. Consider an infinitesimal piece of sphere surface with an area of dS. During a time period of dt, the work done by the movement of dS is:

$$dW = [P(r_0) \times dS] \times [\mathrm{u}(r_0) \times dt] \ . \qquad (Eq.3.36)$$

This is also the energy dissipated dE from the same surface. Thus the instantaneous power radiated from a radially pulsating sphere is:

$$\Pi = \int_S \frac{dE}{dt} = \int_S \frac{[P(r_0) \times dS] \times [\mathrm{u}(r_0) \times dt]}{dt}$$

$$= \int_{dS} P(r_0) \times \mathrm{u}(r_0)\, dS \ . \qquad (Eq.3.37)$$

Substituting Eq. 3.34 and Eq. 3.35 into Eq. 3.37, we obtain

$$\Pi = \int_{dS} [-\omega\rho_0 A \cos(\omega t)] \times \{-\frac{A}{r_0}[\sin(\omega t) + kr_0 \cos(\omega t)]\}\, dS$$

$$= (4\pi {r_0}^2) \frac{A^2 \omega \rho_0}{r_0} \cos(\omega t)[\sin(\omega t) + kr_0 \cos(\omega t)]$$

$$= 4\pi\rho_0 r_0 A^2 \omega \cos(\omega t)[\sin(\omega t) + kr_0 \cos(\omega t)] \ . \qquad (Eq.3.38)$$

The time-averaged power radiated from the radially pulsating sphere is

$$\Pi_{ave} = \frac{\int_T \Pi\, dt}{T} \ . \qquad (Eq.3.39)$$

Substituting Eq. 3.38 into Eq. 3.39, we obtain

$$\Pi_{ave} = (\int_T 4\pi\rho_0 r_0 A^2 \omega \cos(\omega t)[\sin(\omega t) + kr_0 \cos(\omega t)]\, dt)/T$$

$$= \frac{\left[(4\pi\rho_0 r_0 A^2 \omega)\left(\int_T \cos(\omega t)\sin(\omega t)\, dt + kr_0 \int_T \cos^2(\omega t)\, dt\right)\right]}{T} \ .$$

$$(Eq.3.40)$$

The following trigonometric relationships will be used:

$$\frac{1}{T}\int_0^T sin^2\, \omega t dt \ ;$$

$$= \frac{1}{T\omega}\int_0^T \frac{1 - \cos 2(\omega t)}{2} d(\omega t) \ ;$$

$$= \frac{1}{T\omega}[\int_0^T \frac{1}{2} d(\omega t) - \frac{1}{4}\int_0^T \cos 2(\omega t)\, d2(\omega t)] \ ;$$

$$= \frac{1}{T\omega}\left[\frac{1}{2}\omega T + \frac{1}{4}\sin 2(\omega T)\right] \ ;$$

$$= \frac{1}{T\omega}[\frac{1}{2}\omega T + \frac{1}{4}\sin 2(\omega\frac{2\pi}{\omega})] \ ;$$

$$= \frac{\omega T}{2T\omega} = \frac{1}{2} \ . \qquad (Eq.3.41\ a)$$

Other relationships include:

$$\frac{1}{T}\int_0^T \cos^2(\omega t)dt = \frac{1}{2} \ ; \qquad (Eq.3.41\ b)$$

$$\frac{1}{T}\int_0^T \sin(\omega t)\cos(\omega t)dt = 0 \ . \qquad (Eq.3.41\ c)$$

Substituting Eq. 3.41-b and Eq. 3.41-c into Eq. 3.40 and simplifying, we obtain

$$\Pi_{ave} = (4\pi\rho_0 r_0 A^2\omega)\frac{kr_0}{2} = 2\pi k\rho_0 {r_0}^2 A^2\omega \ . \qquad (Eq.3.42)$$

Note the wave number, $k = \omega/c$. Eq. 3.42 is written as

$$\Pi_{ave} = 2\pi k^2 {r_0}^2 \rho_0 c_0 A^2 \ . \qquad (Eq.3.43)$$

The velocity at the surface of the pulsating sphere is given by Eq. 3.34, repeated here:

$$\mathbf{u}(\mathrm{r}_0) = -\frac{A}{r_0}[\sin(\omega t) + kr_0\cos(\omega t)] \ .$$

Since the sphere is vibrating harmonically, the amplitude of the velocity at the surface is basically a sinusoidal function, $\mathbf{u}(\mathrm{r}_0) = u_0\sin(\omega t + \varphi)$. Hence,

$$\mathbf{u}(\mathrm{r}_0) = -\frac{A}{r_0}[\sin(\omega t) + kr_0\cos(\omega t)] = u_0\sin(\omega t + \varphi) \ .$$

That is,

$$-A[\sin(\omega t) + kr_0\cos(\omega t)] = u_0 r_0[\sin\omega t\cos\varphi + \cos\omega t\sin\varphi] \ .$$

By comparing the left side and right side, the amplitude is:

$$A = -u_0 r_0\cos\varphi \ ; \qquad (Eq.3.44\ a)$$

and

$$Akr_0 = -u_0 r_0\sin\varphi \ . \qquad (Eq.3.44\ b)$$

Squaring both Eq. 3.44-a and Eq. 3.44-b,

$$A^2 = (u_0 r_0)^2 \cos^2 \varphi \ , \qquad (Eq. 3.45\ a)$$

$$A^2 (kr_0)^2 = (u_0 r_0)^2 \sin^2 \varphi \ . \qquad (Eq. 3.45\ b)$$

Adding Eq. 3.45-a and Eq. 3.45-b together, we obtain

$$A^2 [1 + (kr_0)^2] = (u_0 r_0)^2 \ .$$

Solving for A^2,

$$A^2 = \frac{(u_0 r_0)^2}{[1 + (kr_0)^2]} \ . \qquad (Eq. 3.46)$$

Substituting Eq. 3.46 into Eq. 3.43 and simplifying, we have the final expression for the time-averaged power radiated from a pulsating sphere:

$$\Pi_{ave} = 2\pi {r_0}^2 {u_0}^2 \rho_0 c_0 \frac{(kr_0)^2}{1 + (kr_0)^2} \ . \qquad (Eq. 3.47)$$

In Eq. 3.47, when $kr_0 \gg 1$, the vibrational frequency is relatively high and the wave length is much smaller that the dimension of the sphere. The power radiated per unit surface area is $\frac{1}{2} {u_0}^2 \rho_0 c_0$. This is the same expression as for radiation to one side from a rigid plate with a vibrational velocity amplitude, u_0.

When $kr_0 \ll 1$, the vibrational frequency is relatively low and the wave length is much larger than the dimension of the sphere. The expression gets close to zero, which means for a vibrating target with a dimension much smaller than the wave length, the efficiency of radiation is low; there is hardly any radiation from the vibrating source. This is referred to as small source vibration, according to Blackstock [2000].

3.4 Radiation from an Oscillating Sphere

Also, according to literature (ANSOL, Advanced Numerical Solutions), the

time-averaged power radiated from a transversely oscillating sphere is derived as:

$$\Pi_{ave} = \frac{2\pi}{3} {r_0}^2 {u_0}^2 \rho_0 c_0 \frac{(kr_0)^4}{4 + (kr_0)^4} \ . \qquad (Eq. 3.48)$$

3.5 Radiation Efficiency

Eq. 3.47 shows that the radiated power is low when the vibrational frequency is very low ($kr_0 \ll 1$), and the radiated power is high when the vibrational frequency is very high ($kr_0 \gg 1$). To understand this idea, the following study is performed.

The pressure at the surface of the sphere is given by Eq. 3.35, repeated here:

$$P(r_0) = -\omega \rho_0 A \cos(\omega t) \ , \qquad (Eq. 3.35)$$

where A is given by Eq. 3.45(a), repeated here:

$$A^2 = (u_0 r_0)^2 \cos^2 \varphi \ , \qquad (Eq. 3.45\ a)$$

Substituting Eq. 3.45(a) into Eq. 3.35, the pressure at the surface of a pulsating sphere can be written as:

$$P(r_0) = -\omega \rho_0 u_0 r_0 \cos\varphi \cos(\omega t) \ . \qquad (Eq. 3.49)$$

The velocity at the surface of the sphere is given by Eq. 3.34, repeated here:

$$\mathbf{u}(\mathrm{r}_0) = -\frac{A}{r_0}[\sin(\omega t) + kr_0 \cos(\omega t)] \ . \qquad (Eq. 3.34)$$

The displacement at the surface of the sphere is obtained by integrating Eq. 3.34 over time, t:

$$\mathrm{d}(\mathrm{r}_0) = -\frac{\cos\varphi}{r_0}\left[-\frac{1}{\omega}\cos(\omega t) + \frac{kr_0}{\omega}\sin(\omega t)\right] \ . \qquad (Eq. 3.50)$$

In Eq. 3.49 and Eq. 3.50, r_0 is the radius of the sphere, u_0 is the amplitude of vibrational speed, and ρ_0 is the density of air.

From Eq. 3.45 (a) and Eq. 3.45 (b), we can solve for φ as:

$$\varphi = \tan^{-1}(\pm\frac{1}{kr_0}) \ , \qquad (Eq. 3.51)$$

thus when

$$kr_0 \gg 1, \varphi \approx \tan^{-1}(0) = 0 \ ;$$

$$\cos\varphi = 1 \ ; \qquad (Eq.3.52)$$

when

$$kr_0 \ll 1, \varphi \approx \tan^{-1}(\infty) = \frac{\pi}{2} \ ;$$

$$\cos\varphi = 0 \ . \qquad (Eq.3.53)$$

Since the energy radiated from the pulsating sphere approximately equals to the work done by the moving of the surface of the sphere, that is,

$$E \approx \frac{1}{T}\int_T P(r_0) \times \mathrm{d}(\mathrm{r}_0)\, dt \ . \qquad (Eq.3.54)$$

Substituting Eq. 3.52 into Eq. 3.54, when the frequency is high, the energy dissipated from the sphere is:

$$E \approx \frac{1}{T}\int_T P(r_0) \times \mathrm{d}(\mathrm{r}_0)\, dt$$

$$= \frac{1}{T}\int_T [-\omega\rho_0 u_0 r_0 \cos(\omega t)] \times \left\{-\frac{1}{r_0}\left[-\frac{1}{\omega}\cos(\omega t) + \frac{kr_0}{\omega}\sin(\omega t)\right]\right\} dt$$

$$\neq 0 \ .$$

On the other hand, substituting Eq. 3.53 into Eq. 3.54, when the frequency is low, the energy dissipated from the sphere is:

$$E \approx \frac{1}{T}\int_T P(r_0) \times \mathrm{d}(\mathrm{r}_0)\, dt$$

$$\approx \frac{1}{T}\int_T [-\omega\rho_0 u_0 r_0(0) \cos(\omega t)] \times \left\{-\frac{0}{r_0}\left[-\frac{1}{\omega}\cos(\omega t) + \frac{kr_0}{\omega}\sin(\omega t)\right]\right\} dt$$

$$= 0 \ .$$

This explains why the acoustic energy radiation is low at low frequencies.

In this chapter we have derived the expression for acoustic radiation from a pulsating sphere and an oscillating sphere. A study was performed to help us understand why acoustic radiation is low under low frequencies, and why it is high under high frequencies. Eq. 3.47 and Eq. 3.48 will be related to damping based on energy radiation in the next chapter. In the next chapter, an equivalent damping ratio will be derived based upon the radiated acoustic energy from a vibrating target.

CHAPTER 4.

ACOUSTIC DAMPING OF SPHERES

4.1 General

Buildings and elements of buildings are immersed in air, and this air has an effect upon the vibrations, especially upon the transmission of vibrational energy from machinery to a building's walls and roofs. The interaction between the solid structure and the air may need to be taken into consideration in modeling building vibrations.

There is a fundamental difference between the vibrational character of air enclosed within a structure and the vibrational character of air surrounding the structure. Ortega [2008] has shown in previous work that the enclosed air has the effect of altering structural modes of vibration and even adding new modes of vibration. Although air has an intrinsic damping effect in which acoustic energy is converted to heat, this effect is minor and thus the damping effect of the enclosed air is ignored in this thesis.

On the other hand, air surrounding the building radiates vibrational energy away from the structure, and this radiated energy is lost from the building system. To understand the damping effect of this radiated energy, we conduct the following study.

4.2 Equivalent Damping Coefficient based on Pulsating Sphere

A simple system is shown in Fig. 4.1. A pulsating sphere is modeled as a spring-mass system with enclosed and surrounding air. The pulsating surface of the sphere can be modeled as an infinite number of infinitesimal spring-mass systems.

Each of the infinitesimal spring mass systems has a vibrating mass, m_0, and a spring stiffness, k_0. For the whole system, we assume the total lumped mass, m, includes inside air, and the total spring stiffness is k. The effect of inside air on the mass is also included in the spring stiffness. After an initial displacement, Δ_0, the whole system undergoes free vibration without damping (except by interaction with the air), and energy is lost from the spring-mass system as vibrational energy is dissipated into the surrounding air.

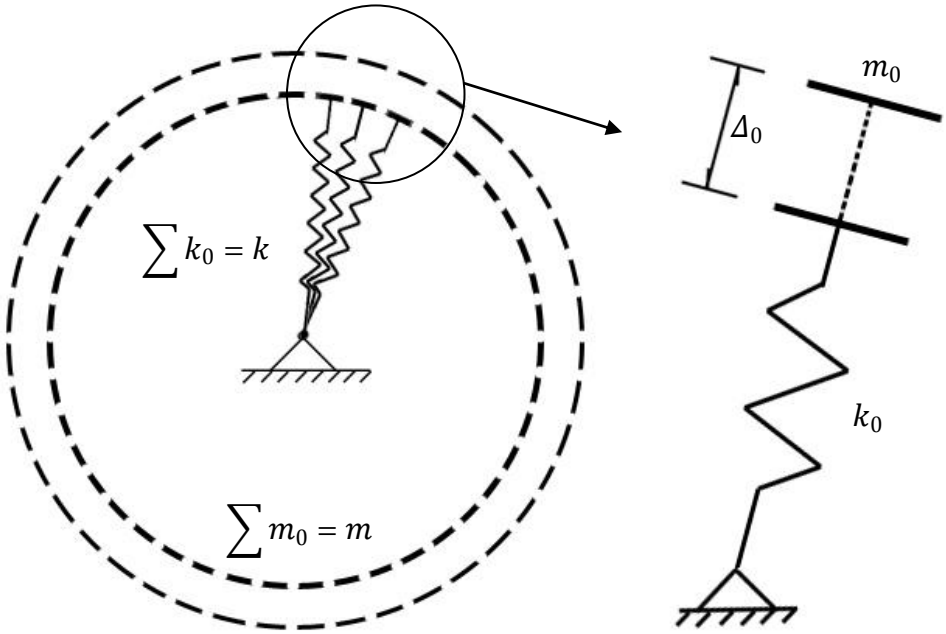

Fig. 4.1: A Spring-Mass System Simulating the Behavior of a Pulsating Sphere

The total initial potential energy, E_0, of the system is:

$$E_0 = \frac{1}{2} k {\Delta_0}^2 \ . \qquad (Eq. 4.1)$$

Assuming the damping of the air is below critical, the displacement, Δ, and velocity, u, are approximately:

$$\Delta \simeq \Delta_0 \cos \omega t \qquad (Eq. 4.2)$$

$$u \simeq -\Delta_0 \omega \sin \omega t \qquad (Eq. 4.3)$$

Eq. 3.47 has shown that the time-averaged power radiated from a pulsating sphere is given as:

$$\Pi_{ave} = 2\pi {r_0}^2 {u_0}^2 \rho_0 c_0 \frac{(kr_0)^2}{1+(kr_0)^2} \ . \qquad (Eq. 4.4)$$

where $2\pi {r_0}^2$ can be written as $A/2$, which is half of the surface area of the sphere. Thus, Eq. 4.4 can be written as:

$$\Pi_{ave} = \frac{A}{2} {u_0}^2 \rho_0 c_0 \frac{(kr_0)^2}{1+(kr_0)^2} \ . \qquad (Eq. 4.5)$$

The energy dissipated per cycle due to acoustic radiation is obtained by multiplying Eq. 4.5 by the period, T:

$$E_{cycle} = \frac{A}{2} {u_0}^2 \rho_0 c_0 \frac{(kr_0)^2}{1+(kr_0)^2} T \ . \qquad (Eq. 4.6)$$

The model in Fig. 4.1 is assumed to be undergoing free vibration without damping. Only acoustic energy radiation is present. Now we find the equivalent damping coefficient in this system by looking at an equivalent viscously damped system, as shown in Fig. 4.2.

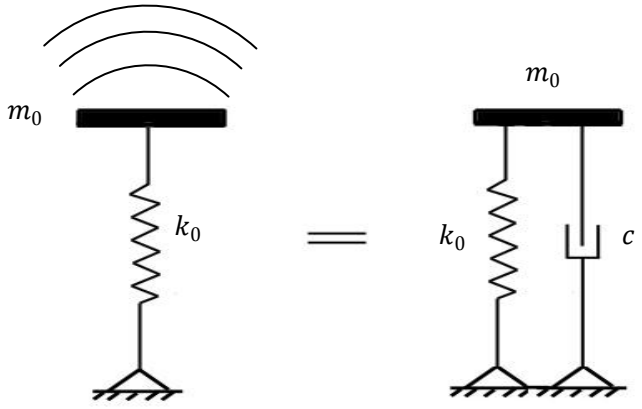

Fig. 4.2: Air-Damped System is Equated to a System with Damper, c.

Chopra [2007] has shown that for a system with viscous damping, the energy dissipated from time 0 to time t is :

$$E_D = \int f_D d\Delta = \int_0^t (c\,u) u dt = \int_0^t c u^2 dt \ . \qquad (Eq.\,4.7)$$

where c is the damping coefficient, u is the velocity function and f_D is the damping force. Substituting the speed function Eq. 4.3 into Eq. 4.7, the total energy dissipated due to damping is approximately:

$$E_D = \int_0^t c(-\Delta_0 \omega \sin \omega t)^2 dt \ . \qquad (Eq.\,4.8)$$

For one full vibration cycle, $t = T$, the energy dissipated due to damping over one time period T is:

$$E_D = \int_0^T c(-\Delta_0 \omega \sin \omega t)^2 dt$$

$$= c(\Delta_0 \omega)^2 \int_0^T \sin^2 \omega t \, dt$$

$$= \frac{1}{2} c(\Delta_0 \omega)^2 T \ . \qquad (Eq.\,4.9)$$

Eq. 4.9 is approximately the energy dissipated per cycle of the system under free vibration with viscous damping. To find the equivalent damping coefficient for the air-damped system, let Eq. 4.9 equal Eq. 4.6:

$$E_D = E_{cycle} \ .$$

That is,

$$E_D = \frac{1}{2} c(\Delta_0 \omega)^2 T = \frac{A}{2} {u_0}^2 \rho_0 c_0 \frac{(kr_0)^2}{1 + (kr_0)^2} T = E_{cycle} \ . \quad (Eq.\,4.10)$$

Note that c_0 is the sound speed while c is the damping coefficient for a viscously damped system. We may want to write the damping coefficient, c, as c_{eq} because it is the equivalent damping coefficient for the air-damped system.

Thus Eq. 4.10 becomes:

$$E_D = \frac{1}{2} c_{eq} (\Delta_0 \omega)^2 T = \frac{A}{2} {u_0}^2 \rho_0 c_0 \frac{(kr_0)^2}{1 + (kr_0)^2} T = E_{cycle} \quad . (Eq. 4.11)$$

Solving Eq. 4.11 for c_{eq}:

$$c_{eq} = \rho_0 c_0 A \frac{(kr_0)^2}{1 + (kr_0)^2} . \qquad (Eq. 4.12)$$

This is the form of the equivalent damping coefficient for a pulsating sphere. The critical damping coefficient c_{cr} is defined by $c_{cr} = 2\sqrt{km} = 2\omega m$. Based on Eq. 4.12, the equivalent damping ratio is found to be:

$$\xi_{eq} = \frac{c_{eq}}{c_{cr}} = \frac{\rho_0 c_0 A}{2\omega m} \frac{(kr_0)^2}{1 + (kr_0)^2} \quad . \qquad (Eq. 4.13)$$

This is the expression for the equivalent damping coefficient due to radiated acoustic energy from a pulsating sphere.

4.3 Equivalent Damping Coefficient Based on Oscillating Sphere

Eq. 3.48 has shown that the time-averaged power radiated from a transversely oscillating sphere is given as:

$$\Pi'_{ave} = \frac{2\pi}{3} {r_0}^2 {u_0}^2 \rho_0 c_0 \frac{(kr_0)^4}{4 + (kr_0)^4} \quad . \qquad (Eq. 4.14)$$

Going through the same procedure as in section 4.2, the equivalent damping coefficient due to radiated acoustic energy from an oscillating sphere is found to be:

$$\xi'_{eq} = \frac{\rho_0 c_0 A}{6\omega m} \frac{(kr_0)^4}{4 + (kr_0)^4} \quad . \qquad (Eq. 4.15)$$

The differences between Eq. 4.13 and Eq. 4.15 are:

(1) A pulsating sphere is approximately equivalent to a baffled piston. Thus, Eq. 4.13 can be applied to a baffled vibrating plate to calculate its damping ratio because it assumes the propagation of acoustic wave is radial, which is close to the acoustic wave from a pulsating sphere, at least in the far-field.

(2) An oscillating sphere is approximately equivalent to an un-baffled piston.

Thus, Eq. 4.15 can be applied to an un-baffled vibrating plate to calculate its damping ratio because the propagation of acoustic wave is non-radial, which is close to the acoustic wave from an oscillating sphere.

Eq. 4.13 and Eq. 4.15 will be used later to predict the damping ratios of several experimental devices. The results will be compared with test results.

In summary, using acoustic theory, we have determined the expressions for damping ratios based on both a pulsating and an oscillating sphere. We will use these expressions to make approximate models of vibrating buildings.

CHAPTER 5.

ENERGY DISSIPATION : FLUID DYNAMICS THEORY

5.1 General

In chapter 4 the damping effect of a system due to acoustic radiation was calculated. This calculation assumes the energy lost is purely caused by acoustic power radiation. As stated in chapter 2, acoustic theory assumes that the fluid in which the vibrating target is immersed has small particle motions. On the other hand, the fluid dynamics theory used in this thesis assumes that the fluid has large particle displacements, and the fluid has a steady flow velocity. For a vibrating target, the air flow around it is not steady. However it can be assumed to be steady when the vibrational frequency is low and the particle displacement is much larger than the dimension of the target.

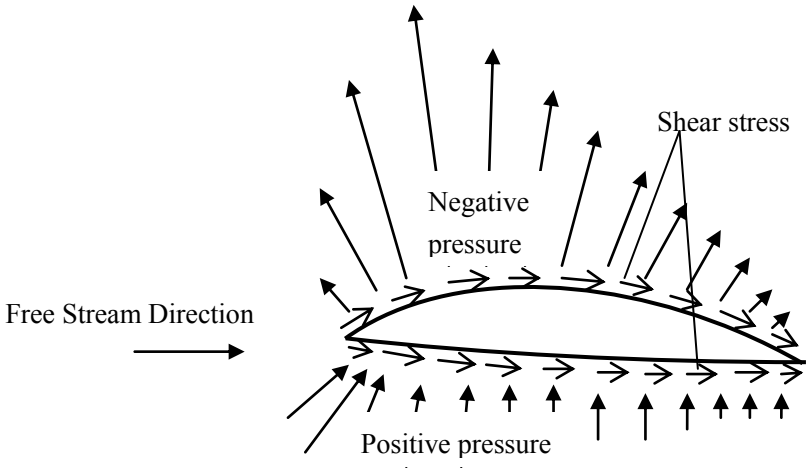

Fig. 5.1: Pressure and Shear Stress on a Wing

Fluid dynamics theory assumes that structures immersed in a flowing fluid like air are under both pressure and viscous forces from the fluid. The sum of the pressure

and the viscous force is divided into two parts. The force that acts normal to the free-stream direction is the lift; the force that acts parallel to the free-stream direction is the drag. This concept is shown in Fig. 5.1. The high speed of flow over the top of the airfoil causes a negative pressure on the top surface. On the bottom surface, the low speed of flow causes a positive pressure. The negative pressure over the top and the positive pressure under the bottom contribute to the lift. The shear stress which is parallel to the surface contributes largely to the drag.

For a uniform vibrating target, the air flow around the target causes the drag force. The work done by the drag force could cause energy to be lost. In this chapter, analytical solutions for energy lost due to drag force will be derived to compare with the energy lost due to acoustic radiation.

5.2 Drag of Bodies

The general analytical solution for lift and drag can be derived by looking at a differential area on the bottom surface of the airfoil shown in Fig. 5.2.

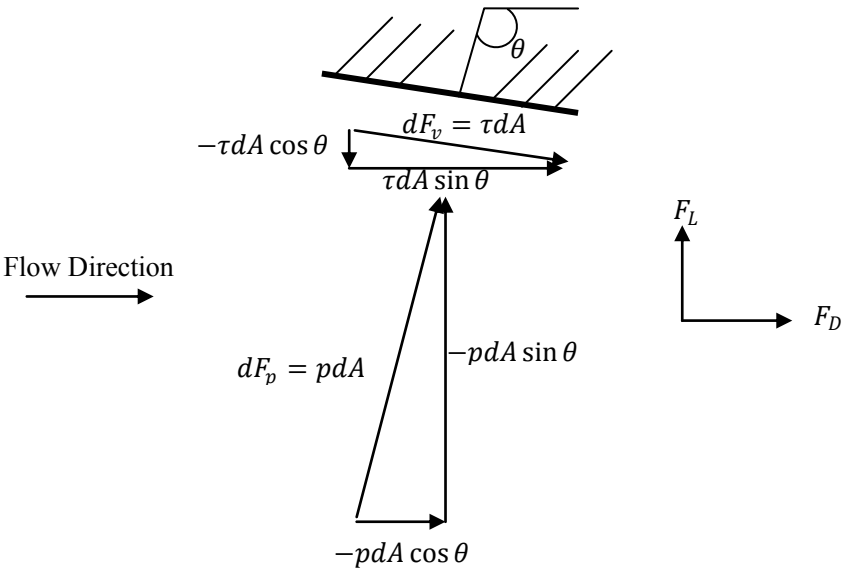

Fig. 5.2: Pressure and Viscous Forces on a Differential Area

In Fig. 5.2, the magnitude of pressure force is $dF_p = pdA$ and the magnitude of viscous force is $dF_v = \tau dA$. F_L and F_D are the lift and drag. Thus, from trigonometric relationships, we have

$$dF_L = -pdA\sin\theta - \tau dA\cos\theta \ , \qquad (Eq.5.1)$$

and

$$dF_D = -pdA\cos\theta + \tau dA\sin\theta \ . \qquad (Eq.5.2)$$

Integrating Eq. 5.1 and Eq. 5.2 over the entire surface of the air foil A, we obtain the total lift force and drag as:

$$F_L = \int(-pdA\sin\theta - \tau dA\cos\theta)dA \ , \qquad (Eq.5.3)$$

and

$$F_D = \int(-pdA\cos\theta + \tau dA\sin\theta)\,dA \ . \qquad (Eq.5.4)$$

5.3 Drag of Thin Plate

Consider a thin plate that is placed normal to a fluid flow, shown in Fig. 5.3. The plate has dimensions of $B \times l$; the thickness is neglected.

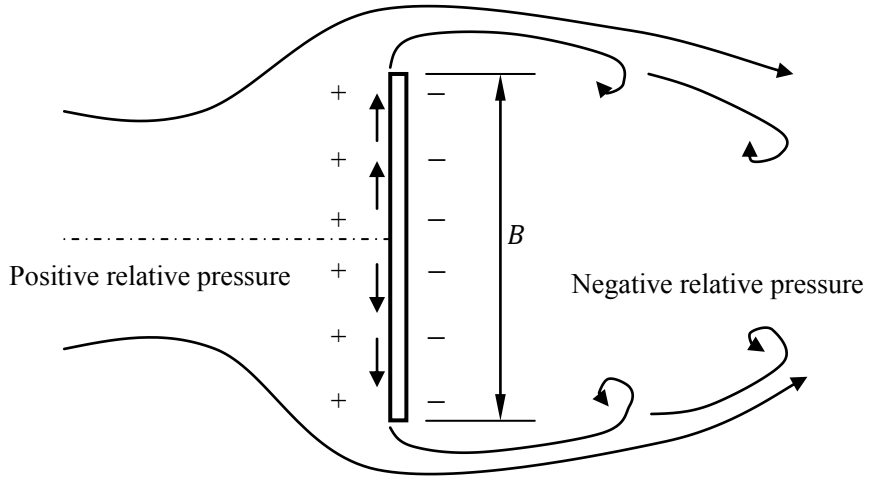

Fig. 5.3: Plate Normal to Air Flow

When the plate is normal to the flow, the viscous forces act symmetrically about the centerline of the plate and are in opposite directions. Thus they do not contribute to either lift or drag. Only the pressure force contributes to the drag. Eq. 5.4 is then written as:

$$F_D = \int (-pdA\cos\theta)\, dA \ . \qquad (Eq.5.5)$$

Roberson and Crowe [1975] showed that, with certain assumptions, the pressure on the rear side of the plate is constant and is given as

$$p = p_0 - 1.2\rho\frac{{V_0}^2}{2} \ . \qquad (Eq.5.6)$$

where p_0 is the free-stream pressure, ρ is the density of the fluid, and V_0 is the free-stream speed. According to Fig. 5.2, θ is the angle from the free-stream direction to the pressure force direction. For the rear side, $\theta = 0$. The contribution to drag for the rear side is

$$F_{D,rear} = -\left(p_0 - 1.2\rho\frac{{V_0}^2}{2}\right)Bl \ . \qquad (Eq.5.7)$$

For the front side, $\theta = \pi$.

$$F_{D,front} = \int_{-B/2}^{B/2}\left(p_0 + C_p\rho\frac{{V_0}^2}{2}\right)l\, dy \ . \qquad (Eq.5.8)$$

where C_p is the average pressure coefficient over the front side. The total drag is the summation of drag on both rear side and front side. After simplification, we obtain:

$$F_D = F_{D,rear} + F_{D,front} = \rho\frac{{V_0}^2}{2}l\left(\int_{-\frac{B}{2}}^{\frac{B}{2}} C_p\, dy + 1.2B\right) . \qquad (Eq.5.9)$$

where $\int_{-\frac{B}{2}}^{\frac{B}{2}} C_p\, dy$ is given as $0.8B$ for a thin plate. Thus Eq. 5.9 is simplified as

$$F_D = 2\rho{V_0}^2 lB \ . \qquad (Eq.5.10)$$

According to Roberson and Crowe [1975], the parameter in the parenthesis in Eq. 5.9 varies with different shapes. Thus it is redefined as C_D, which is called the coefficient of drag. Eq. 5.9 is rewritten in a more general manner:

$$F_D = C_D A_p \rho \frac{{V_0}^2}{2} \ . \qquad (Eq. 5.11)$$

where A_p is the projected area of the body.

For example, for a specific rectangular plate with $l/B = 1$, $C_D = 1.18$. Thus we obtain the drag force for a square plate placed normal to the fluid flow as

$$F_D = 0.59 A_p \rho {V_0}^2 \ . \qquad (Eq. 5.12)$$

5.4 Power Dissipated Due to Drag

Consider a target vibrating with such a low frequency that the air flowing around the target is assumed to have a steady flow velocity, and we assume that fluid dynamics theory applies. Remember that for a vibrating target, the displacement and velocity are given in Eq. 4.2 and Eq. 4.3 as

$$\Delta \simeq \Delta_0 \cos \omega t \ , \qquad (Eq. 4.2)$$

$$\mathrm{u} \simeq -\Delta_0 \omega \sin \omega t \ . \qquad (Eq. 4.3)$$

For one cycle, the work done by drag is:

$$W_D = \int_0^T (F_D)(\mathrm{u})\mathrm{dt} = -4 \int_0^{\frac{T}{4}} \left(C_D A_p \rho \frac{{V_0}^2}{2} \right) (\Delta_0 \omega \sin \omega t)\mathrm{dt} \ . \quad (Eq. 5.13)$$

If we assume the speed of the vibrating target is time-averaged:

$$V_0 = \left| \frac{1}{T} \int_0^T u \, dt \right| = \left| \frac{1}{T} \int_0^T (-\Delta_0 \omega \sin \omega t) \, dt \right| = \frac{\Delta_0}{T} \ . \qquad (Eq. 5.14)$$

Substituting Eq. 5.14 into Eq. 5.13 and simplifying, the work done by drag in one cycle is:

$$W_D = 2C_D A_p \rho \frac{{\Delta_0}^3}{T^2} \ . \qquad (Eq. 5.15)$$

Eq. 5.15 is the energy lost in one cycle of vibration. Now according to Eq. 4.13, the energy dissipated due to viscous damping, c, is given by:

$$E_{damp} = \frac{1}{2} c_{eq} (\Delta_0 \omega)^2 T \ . \qquad (Eq. 5.16)$$

To find the equivalent damping coefficient for drag, let Eq. 5.15 equal Eq. 5.16. Thus,

$$2C_D A_p \rho \frac{{\Delta_0}^3}{T^2} = \frac{1}{2} c_{eq} (\Delta_0 \omega)^2 T \ .$$

Solving for c_{eq} and simplifying, we obtain:

$$c_{eq} = \frac{1}{\pi^2} C_D A_p \rho \Delta_0 f \ . \qquad (Eq. 5.17)$$

where f is the vibrational frequency with a unit of hertz.

Writing the density of air as ρ_0, and the area of the vibrating target as A, the damping ratio for a vibrating plate based on drag is then:

$$\xi''_{eq} = \frac{c_{eq}}{c_{cr}} = \frac{1}{4\pi^3} \frac{C_D A \rho_0 \Delta_0}{m} \ , \qquad (Eq. 5.18)$$

where c_{cr} has been previously defined as the critical damping coefficient, $c_{cr} = 2\omega m$, where m is the mass of the vibrating target. This equation will be used later to calculate the damping ratio based on experimental devices. The result will then be compared with test results.

Now we have related the energy dissipation based on fluid dynamic theory to the damping effect upon a structure. Eq. 5.18 is derived by equalizing the energy lost from a viscously damped system to the work done by the drag force caused by a steady fluid flow. However, the vibrational frequency range should be low enough for the structure's average vibrational speed to be approximated by the steady fluid flow

speed, which generates the viscous forces acting symmetrically about the central line of the plate (shown in Fig. 5.3). The fluid flow shown in Fig. 5.3 causes fluid transportation from one side of the plate to the other, which is called fluid convection. If the vibrational frequency is so high that there is not enough time for the fluid to be transported back and forth, then drag cannot be generated, and rotational flow cannot emerge and the vibrating structure generates plane waves. In this case fluid dynamics theory no longer applies. Therefore, we expect Eq. 5.18 is applicable to low-frequency oscillatory vibration.

On the other hand, the equivalent damping ratio based on acoustic theory (Eq. 4.15, Eq. 4.17) was derived by equalizing the energy lost from a viscously damped system to the acoustic power radiated from either a pulsating sphere or an oscillating sphere. To apply these two equations, we expect the vibrational frequency should be high enough for structures to generate sound so that acoustic radiation exists.

The question of when fluid dynamics theory governs behavior and when acoustic theory governs behavior is deferred to chapter 10.

The next chapter presents theoretical acoustic solutions for a baffled piston.

CHAPTER 6.

A BAFFLED PISTON : RAYLEIGH INTEGRAL SOLUTION

6.1 General

To this point, we have studied the acoustic air-damping effect of a pulsating sphere and an oscillating sphere; the equivalent damping ratio can also be calculated using Eq. 5.18, which is based on fluid dynamics theory. All these equations are repeated here.

$$\xi_{eq} = \frac{\rho_0 c_0 A}{2\omega m} \frac{(kr_0)^2}{1+(kr_0)^2} \; ; \qquad (Eq. 4.13)$$

$$\xi'_{eq} = \frac{\rho_0 c_0 A}{6\omega m} \frac{(kr_0)^4}{4+(kr_0)^4} \; ; \qquad (Eq. 4.15)$$

$$\xi''_{eq} = \frac{1}{4\pi^3} \frac{C_D A \rho_0 \Delta_0}{m} \, , \qquad (Eq. 5.18)$$

We have looked at two opposite extremes where either high-frequency vibration (which generates acoustic radiation) or low-frequency vibration (which generates rotational fluid convection) applies, respectively. To understand how important the fluid flow's influence is, we are now interested in the behavior of a vibrating structure with little fluid convection, as a comparison. For such a study, we now consider the vibration of a baffled piston.

A baffled piston is an infinite plane (the baffle) except for a section (the piston), which vibrates normal to the plane. The purpose of the baffle is to restrict the sound field to only one direction. In this chapter, we will derive the analytical solution for the baffled piston, which is called the Rayleigh Integral. The solution will be compared with experimental results in subsequent chapters.

6.2 Analytical Solution for Rayleigh Integral

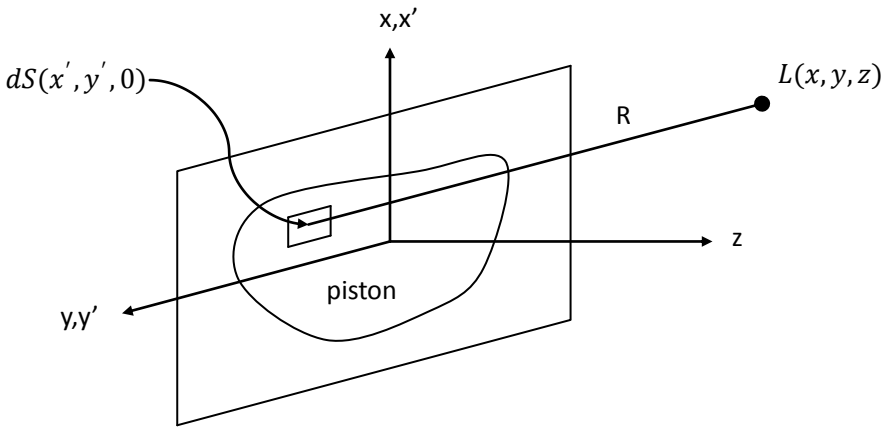

Fig. 6.1: Baffled Piston of Arbitrary Shape

Fig. 6.1 shows the concept of radiation from a baffled piston of arbitrary shape. Blackstock [2000] has shown in his book *Fundamentals of Physical Acoustics* that the pressure field produced by a vibrating piston mounted in a baffle is given as:

$$p(x, y, z; t) = \rho_0 \int_S \frac{\dot{u}_p\left(x^{'}, y^{'}; t - \frac{R}{c_0}\right)}{2\pi R} dS \ . \qquad (Eq. 6.1)$$

where ρ_0 is the static density of medium around the vibrating source, and c_0 is the speed of sound in that medium. $x^{'}$ and y' are the coordinates of the source point on the piston, $\dot{u}_p$ is the piston's acceleration, and *S* is the area of the vibrating piston. *R* is the distance from $(x^{'}, y^{'})$ on the piston to the point (x, y, z) of interest, and is written as:

$$R = \sqrt{(x - x^{'})^2 + (y - y^{'})^2 + z^2} \ . \qquad (Eq. 6.2)$$

Now assuming the piston vibration is harmonic, the speed of the vibrating piston is in the form:

$$u_p = u_0 e^{j\omega t} \ . \qquad (Eq. 6.3)$$

where u_0 is the amplitude of particle velocity, and j is $\sqrt{-1}$. Eq. 6.3 is basically a trigonometric function which is written in complex form for convenience. The

numerator in the integral of Eq. 6.1 can be rewritten as:

$$\begin{aligned}
&\dot{u}_p\left(x^{'}, y^{'}; t-\frac{R}{c_0}\right) \\
&= \frac{d}{dt}\left[u_0 e^{j\omega\left(t-\frac{R}{c_0}\right)}\right] \\
&= \frac{d}{dt}\left[u_0 e^{j\omega t-\frac{j\omega R}{c_0}}\right] \\
&= j\omega u_0 e^{j\omega t-\frac{j\omega R}{c_0}} \ . \qquad (Eq.\,6.4)
\end{aligned}$$

Substituting Eq. 6.4 into Eq. 6.1, the pressure is rewritten as:

$$\begin{aligned}
p(x,y,z;t) &= \rho_0 \int_S \frac{j\omega u_0 e^{j\omega t-\frac{j\omega R}{c_0}}}{2\pi R} dS \\
&= \frac{\rho_0 j\omega u_0 e^{j\omega t}}{2\pi} \int_S \frac{e^{-j\frac{\omega}{c_0}R}}{R} dS \ . \qquad (Eq.\,6.5)
\end{aligned}$$

Defining the wave number k as:

$$k = \frac{\omega}{c_0} \ ,$$

Eq. 6.5 becomes:

$$\begin{aligned}
p(x,y,z;t) &= \frac{\rho_0 j\omega u_0 e^{j\omega t}}{2\pi} \int_S \frac{e^{-j\frac{\omega}{c_0}R}}{R} dS \\
&= \frac{jk\rho_0 c_0 u_0 e^{j\omega t}}{2\pi} \int_S \frac{e^{-jkR}}{R} dS \ . \qquad (Eq.\,6.6)
\end{aligned}$$

This is the general expression for the pressure field caused by a vibrating baffled piston.

6.3 Ring Piston Example

Two examples are cited to illustrate the use of Eq. 6.6. Consider a ring piston having an average radius, a, and a thickness, w, as shown in Fig. 6.2.

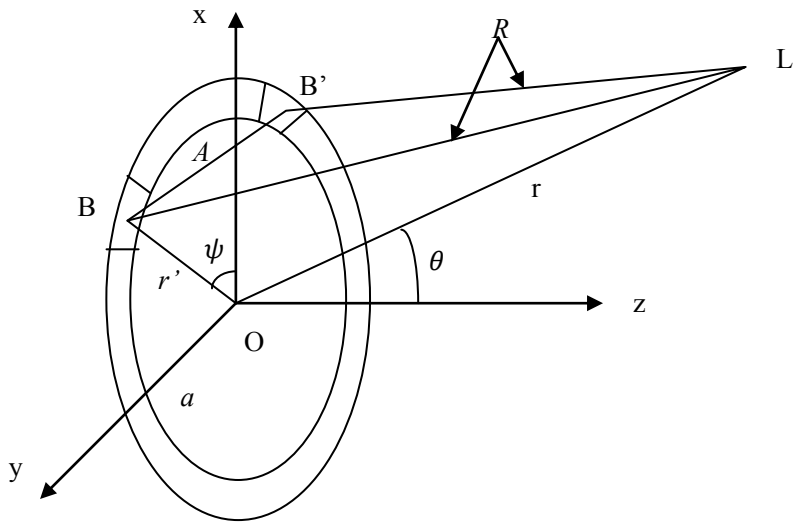

Fig. 6.2: Ring Piston

With reference to Fig. 6.2, r is the vector from the center point O to point L. Assume L is located in the x-z plane.Thus,

$$r = ix + j0 + kz = ir\sin\theta + kr\cos\theta \ .$$

Letting *r'* be the vector from the center O to point B, similarly:

$$r^{'} = ix^{'} + jy^{'} + k0 = ia\cos\psi + ja\sin\psi \ ,$$

and the distance R becomes:

$$R = |r - r^{'}| = \sqrt{r^2 + a^2 - 2ra\sin\theta\cos\psi} \ . \qquad (Eq.\,6.7)$$

In the same manner, another point *B'* mirrored through the x-axis has the same distance *R* to the field point *L*. The two elements at *B*' and *B* has a combined area of:

$$dS = 2awd\psi \ . \qquad (Eq.\,6.8)$$

Substituting Eq. 6.8 into Eq. 6.6, for the ring piston, we obtain:

$$p(x,y,z;t) = \frac{jkaw\rho_0 c_0 u_0 e^{j\omega t}}{\pi}\int_0^{\pi}\frac{e^{-jkR}}{R}d\psi \ . \qquad (Eq.\,6.9)$$

When considering the pressure at far field ($r \gg a$), Eq. 6.7 is written in the form:

$$R = r\left[1 - \left(\frac{a}{r}\right)\sin\theta\cos\psi + 0\left(\frac{a}{r}\right)^2\right]. \qquad (Eq.6.10)$$

Neglecting the higher-order term, we obtain:

$$R = r - a\sin\theta\cos\psi \ . \qquad (Eq.6.11)$$

Substituting Eq. 6.11 into Eq. 6.9, and assuming R in the denominator equals r, we obtain:

$$p(x,y,z;t) = \frac{jkaw\rho_0 c_0 u_0 e^{j\omega t}}{\pi}\int_0^{\pi}\frac{e^{-jkR}}{R}d\psi$$

$$= \frac{jkaw\rho_0 c_0 u_0 e^{j\omega t}}{\pi r}\int_0^{\pi} e^{-jkR}\,d\psi$$

$$= \frac{jkaw\rho_0 c_0 u_0 e^{j\omega t}}{\pi r}\int_0^{\pi} e^{-jk\,(r-a\sin\theta\cos\psi)}d\psi$$

$$= \frac{jkaw\rho_0 c_0 u_0 e^{j\omega t\,-jkr}}{r}\frac{1}{\pi}\int_0^{\pi} e^{jka\sin\theta\cos\psi}d\psi \ . (Eq.6.12)$$

A directional function $J_m(x)$ is defined as follows (Bessel Function):

$$J_m(x) = \frac{j^{-m}}{\pi}\int_0^{\pi} e^{jx\cos\alpha}\cos m\alpha d\alpha \ .$$

Thus the integration term in Eq. 6. 12 can be expressed as:

$$\frac{1}{\pi}\int_0^{\pi} e^{jka\sin\theta\cos\psi}d\psi$$

$$= \frac{\mathrm{j}^{-0}}{\pi}\int_0^{\pi} e^{jka\sin\theta\cos\psi}\cos(0\psi)d\psi$$

$$= J_0(ka\sin\theta) \ . \qquad (Eq.6.13)$$

Substituting Eq. 6.13 into Eq. 6.12 and rewriting:

$$p(x,y,z;t) = \frac{jkaw\rho_0 c_0 u_0}{r}J_0(ka\sin\theta)e^{j\omega t\,-jkr} \ . \qquad (Eq.6.14)$$

This is the approximate expression for calculating the farfield pressure of a baffled ring piston.

6.4 Circular Piston Example

Now, to apply Eq. 6.14 to a circular disk, first, the average ring radius a becomes a variable σ, and the thickness becomes $d\sigma$. Thus, the expression in Eq. 6.8 becomes:

$$dS = 2\sigma d\sigma d\psi \ . \qquad (Eq.6.15)$$

Substituting Eq. 6.15 into Eq. 6.6, we have the general expression for the pressure field of a circular disk:

$$\begin{aligned} p(x,y,z;t) &= \frac{jk\rho_0 c_0 u_0 e^{j\omega t}}{2\pi}\int_S \frac{e^{-jkR}}{R}dS \\ &= \frac{jk\rho_0 c_0 u_0 e^{j\omega t}}{\pi}\int_S \frac{e^{-jkR}}{R}\sigma d\sigma d\psi \\ &= \frac{jk\rho_0 c_0 u_0 e^{j\omega t}}{\pi}\int_0^{\pi} d\psi \int_0^{a} \frac{e^{-jkR}}{R}\sigma d\sigma \ . \end{aligned}$$

$$(Eq.6.16)$$

R is now given by Eq. 6.7, with a replaced by σ. That is:

$$R = \sqrt{r^2 + \sigma^2 - 2r\sigma\sin\theta\cos\psi} \ . \qquad (Eq.6.17)$$

To calculate the farfield radiation, replace *a* and *w* by σ and $d\sigma$ in Eq. 6.14:

$$p(x,y,z;t) = \frac{jk\sigma d\sigma\rho_0 c_0 u_0}{r} J_0(k\sigma\sin\theta) e^{j\omega t - jkr}$$

Integrating over σ:

$$p = \frac{jk\rho_0 c_0 u_0}{r} e^{j\omega t - jkr}\int_0^{a} \sigma J_0(k\sigma\sin\theta) d\sigma \ . \qquad (Eq.6.18)$$

Letting $k\sigma\sin\theta = \mu$, the integration in Eq. 6.18 becomes:

$$\begin{aligned} &\int_0^{a} \sigma J_0(k\sigma\sin\theta) d\sigma \\ &= \int_0^{ka\sin\theta} \frac{\mu}{k\sin\theta} J_0(\mu) d\frac{\mu}{k\sin\theta} \end{aligned}$$

$$= \frac{1}{(k\sin\theta)^2}\int_0^{ka\sin\theta} \mu J_0(\mu)d\mu \ . \qquad (Eq.6.19)$$

Given another Bessel Function:

$$\frac{d}{dx}[x^m J_m(x)] = x^m J_{m-1}(x) \ . \qquad (Eq.6.20)$$

When m=1, Eq. 6.20 becomes:

$$\frac{d}{dx}[xJ_1(x)] = xJ_0(x) \, .$$

Thus, replacing x with μ:

$$\mu J_0(\mu) = \frac{d}{d\mu}[\mu J_1(\mu)] \ . \qquad (Eq.6.21)$$

Substituting Eq. 6.21 into Eq. 6.19, the original integration is simplified as:

$$\frac{1}{(k\sin\theta)^2}\int_0^{ka\sin\theta} \mu J_0(\mu)d\mu$$

$$= \frac{1}{(k\sin\theta)^2}\int_0^{ka\sin\theta} \frac{d}{d\mu}[\mu J_1(\mu)]d\mu$$

$$= \frac{ka\sin\theta J_1(\mu)}{(k\sin\theta)^2} = \frac{a}{ksin\theta}J_1(ka\sin\theta) \, . \qquad (Eq.6.22)$$

Substituting Eq. 6.22 into Eq. 6.18:

$$p = \frac{jk\rho_0 c_0 u_0}{r} e^{j\omega t - jkr} \int_0^a \sigma J_0(k\sigma\sin\theta)d\sigma$$

$$= \frac{jk\rho_0 c_0 u_0}{r} e^{j\omega t - jkr} \frac{a}{k\sin\theta}J_1(ka\sin\theta)$$

$$= \frac{j\rho_0 c_0 u_0 a}{r} \frac{J_1(ka\sin\theta)}{\sin\theta} e^{j\omega t - jkr} \ . \qquad (Eq.6.23)$$

This is the expression to calculate approximate the far-field pressure distribution of a baffled vibrating circular piston.

6.5 Pressure on Central Axis

Now we have derived the expression for farfield pressure due to a vibrating baffled circular disk. We are interested in the pressure value on the central axis normal to the disk surface.

The Bessel Function was previously defined as:

$$J_m(x) = \frac{j^{-m}}{\pi}\int_0^{\pi} e^{jx\cos\alpha}\cos m\alpha d\alpha \ . \qquad (Eq.6.24)$$

Thus, when *m*=0, and $x = ka\sin\theta$

$$J_0(x) = \frac{1}{\pi}\int_0^{\pi} e^{jka\sin\theta\cos\alpha}\cos(0)d\alpha$$

To evaluate the pressure field on central axis, we evaluate the expression when $\theta = 0$:

$$J_0\big(ka\sin(0)\big) = J_0(0) = \frac{1}{\pi}\int_0^{\pi} e^0 d\alpha = 1 \ . \qquad (\text{Eq. } 6.25)$$

Using Eq. 6.20, and letting m=1:

$$\frac{d}{dx}[x^m J_m(x)] = x^m J_{m-1}(x) \ ,$$

and

$$\frac{d}{dx}[xJ_1(x)] = xJ_0(x) \ .$$

Using the result of Eq. 6.25:

$$\frac{d}{dx}[xJ_1(x)] = x$$

$$xJ_1(x) = \frac{x^2}{2}$$

$$J_1(x) = \frac{x}{2} = \frac{ka\sin\theta}{2} \ . \qquad (Eq.6.26)$$

Substituting Eq. 6.26 into Eq. 6.23, Eq. 6.23 is simplified as:

$$\frac{j\rho_0 c_0 u_0 a}{r}\frac{J_1(ka\sin\theta)}{\sin\theta}e^{j\omega t - jkr}$$

$$= \frac{j\rho_0 c_0 u_0 a}{r}\frac{ka}{2}e^{j\omega t - jkr} \ . \qquad (Eq.6.27)$$

Note that this is an evaluation of Eq. 6.23 when $\theta = 0$, which is the pressure field on central axis normal to the disk surface.

The amplitude directivity factor *D* is defined as the pressure at distance R at any angle θ relative to that at $\theta = 0$. Thus:

$$D(\theta) = \frac{p(r,\theta;t)}{p(r,0;t)} = \frac{Eq.23}{Eq.27} = \frac{2J_1(ka\sin\theta)}{ka\sin\theta}$$

Now Eq. 6.23 can be taken in the simpler form:

$$\frac{j\rho_0 c_0 u_0 a}{r}\frac{J_1(ka\sin\theta)}{\sin\theta}e^{j\omega t - jkr} = \frac{j\rho_0 c_0 u_0 a}{2r}D(\theta)e^{j\omega t - jkr} \quad . \qquad (Eq.6.28)$$

The Rayleigh distance is defined in general by

$$R_0 = S/\lambda$$

According to Pierce [1989], S is the piston area and the piston need not necessarily be circular. λ is the wavelength. For the circular piston, $S/\lambda = \pi a^2/\lambda$. Noticing that $k = 2\pi/\lambda$, R_0 is written as:

$$R_0 = ka^2/2$$

Defining $P_0 = \rho_0 c_0 u_0$, Eq. 6.28 is written as:

$$p = j\frac{P_0 R_0}{r}D(\theta)e^{j\omega t - jkr} \quad . \qquad (Eq.6.29)$$

When only the pressure on axis normal to the piston surface is considered,

$$D(\theta) = \frac{p(r,\theta;t)}{p(r,0;t)} = \frac{Eq.23}{Eq.27} = \frac{2J_1(ka\sin\theta)}{ka\sin\theta} = \frac{2\frac{ka\sin\theta}{2}}{ka\sin\theta} = 1$$

Thus, the expression for the amplitude of pressure is written as:

$$p = \frac{P_0 R_0}{r} \, . \qquad (Eq.6.30)$$

This is the final expression for the farfield pressure amplitude along the central

axis normal to the piston surface. P_0 is related to the properties of air and the vibrational speed of the piston, and R_0 is related to the vibrational frequency and the area of the piston.

We have derived the solutions for equivalent damping ratio based on acoustic radiation from both a pulsating sphere and an oscillating sphere; equivalent damping ratio based on fluid dynamics theory; and the solution for the pressure field caused by a baffled circular piston. To evaluate the limitations of applicability of these equations, a series of experiments are conducted. The results of these experiments will be compared with the theoretical solutions. The next three chapters describe the experimental procedures and results.

CHAPTER 7.

UNBAFFLED PLATE EXPERIMENT

7.1 General

In chapter 4 we have derived the expressions for damping ratio of a vibrating target based on theories of acoustic radiation from a pulsating sphere and from an oscillating sphere. Lee [2006] has presented an experiment in which the acceleration histories of a vibrating plate under maximum and minimum air resistance cases are studied. Fig. 7.1 and Fig. 7.2 show the experimental apparatus. The damping ratios of two cases were calculated based on experimental results. The results showed a clear difference between the maximum air resistance case and the minimum air resistance case.

To verify this experiment, in this chapter, a similar vibrating plate experiment will be presented. Since the vibrating plate is unbaffled, the results of the experiment will be compared with damping ratio derived from acoustic theory based on the acoustic radiation from an oscillating sphere, given by Eq. 4.15.

7.2 Experimental Setup – Test 1 ($f_1 = 4.78Hz$)

To observe the difference between a plate vibrating with larger air damping effect and smaller air damping effect, an aluminum plate target supported by a frame consisting of four threaded steel rods is developed, shown in Fig. 7.1. An accelerometer attached to the plate monitors horizontal acceleration. The acceleration response history is processed using the software Labview, in which the Fourier

Transform is computed to help determine the natural frequency.

Fig. 7.1: Plate Target with Frame Support

The four threaded steel rods are bolted to a steel I-beam as a base support. Two square aluminum plates are attached to the steel rods, with one of the plates oriented either horizontally or vertically, as shown in Fig. 7.2. First we start the vibration with the two plates oriented perpendicular to each other. The vertical plate causes a large air damping effect. Then we attach both plates horizontally so that the air damping effect is smaller. Assuming the mass of the aluminum plates is lumped, the structure is approximately a single degree-of-freedom vibrational system.

The weights of the system are shown in Table. 7.1.

Item	Weight (lb)	Total Weight (lb)
Plates	11.163	14.678
Rod Total	3.515	

Table 7.1 : Weights of the System

The dimensions of the system are shown in Fig. 7.2 (a) and Fig. 7.2 (b)

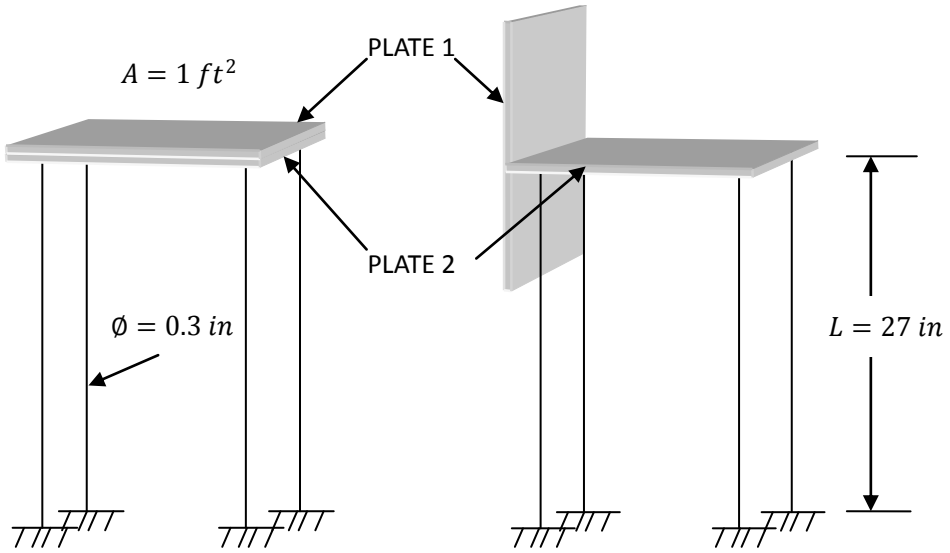

(a): Two Plates Fixed Parallel to Each Other **(b): Two Plates Fixed Normal to Each Other**

Fig. 7.2 : Dimensions of the System

To calculate the natural theoretical natural frequency of the system, assuming the top plate is rigid, the stiffness of a single rod is:

$$k_i = \frac{12EI}{h^3} ,$$

where I is the moment of inertia of the steel rods:

$$I = \frac{\pi d^4}{64} = \frac{(3.14)(0.3\ in)^4}{64} = 3.974 \times 10^{-4}\ in^4$$

Thus,

$$k_i = \frac{12(29000ksi)(3.974 \times 10^{-4} in^4)}{(27in)^3} = 7.026\frac{lb}{in} = 1230.433\frac{N}{m}.$$

The stiffness of the whole system is then:

$$K_1 = 4k_i = 28.104\frac{lb}{in} = 337.248\frac{lb}{ft} = 4921.732\frac{N}{m}.$$

Since the bottom parts of the rods are fixed to the I-beam and these parts do not participate in vibration, assume approximately 14 lb of the system is included in the vibration. The mass of the system is:

$$m_1 = \frac{14\ lb}{32.2\ ft/s^2} = 0.435\ lb \cdot \frac{s^2}{ft} = 6.355\ kg$$

The natural frequency of the system is then found to be:

$$\omega_1 = \sqrt{\frac{K_1}{m_1}} = \sqrt{\frac{337.248\ lb/ft}{0.435\ \frac{lb \cdot s^2}{ft}}} = 27.844 \frac{rad}{s}$$

$$f = 27.844 \frac{rad}{s} = 4.434\ Hz$$

7.3 Acceleration Measurement and Test Results – Test 1 ($f_1 = 4.78Hz$)

An accelerometer is attached to the plate to measure the plate's horizontal acceleration. The acceleration response histories for large damping and small damping are measured separately. For each case, an initial displacement is applied. Then the plate is released, causing free vibration. The initial displacements are measured as 0.125 inch and 0.25 inch, respectively.

Fig. 7.3 shows the large damping case. Fig. 7.4 shows the small air-damping case.

Fig. 7.3 : Vibrational System With Plates Fixed Normal to Each Other. Assuming Large Air-Damping Effect.

Fig. 7.4 : Vibrational System With Plates Fixed Parallel to Each Other. Assuming Small Air-Damping Effect.

The results from the test are plotted and shown in Figs. 7.5 and Fig. 7.6. The tested natural frequency is 4.78 Hz, which is close to the theoretical value of 4.43 Hz.

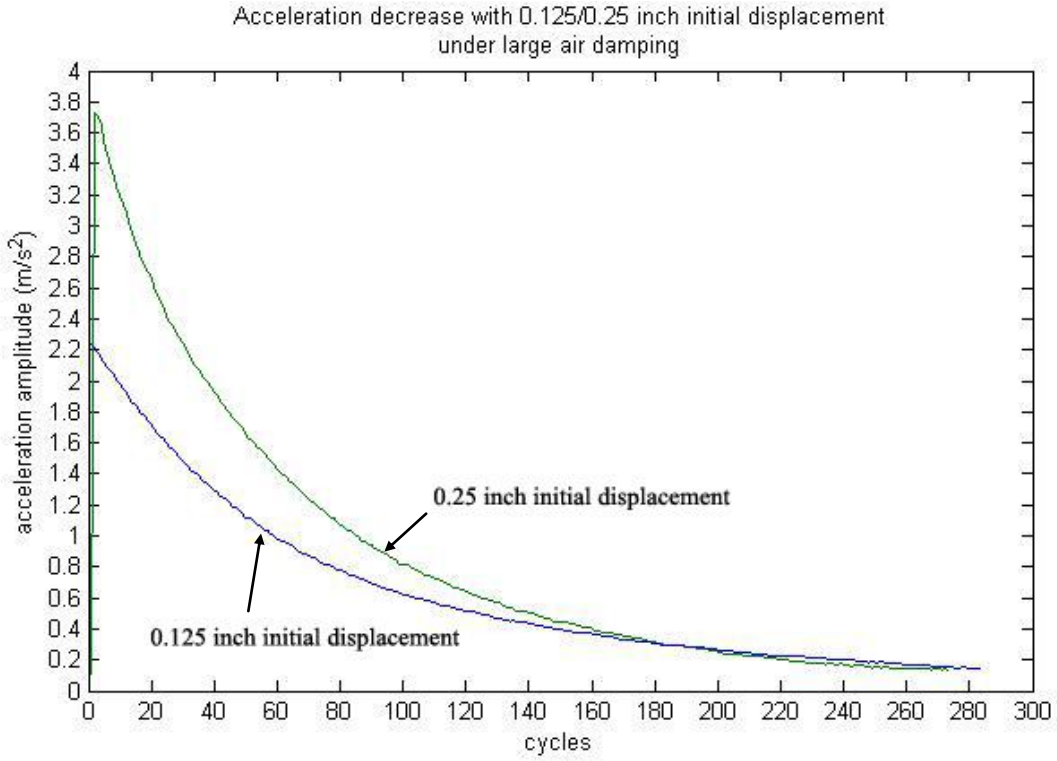

Fig. 7.5 : Acceleration History For Large Air Damping Under both 0.125 Inch and 0.25 Inch Initial Displacement

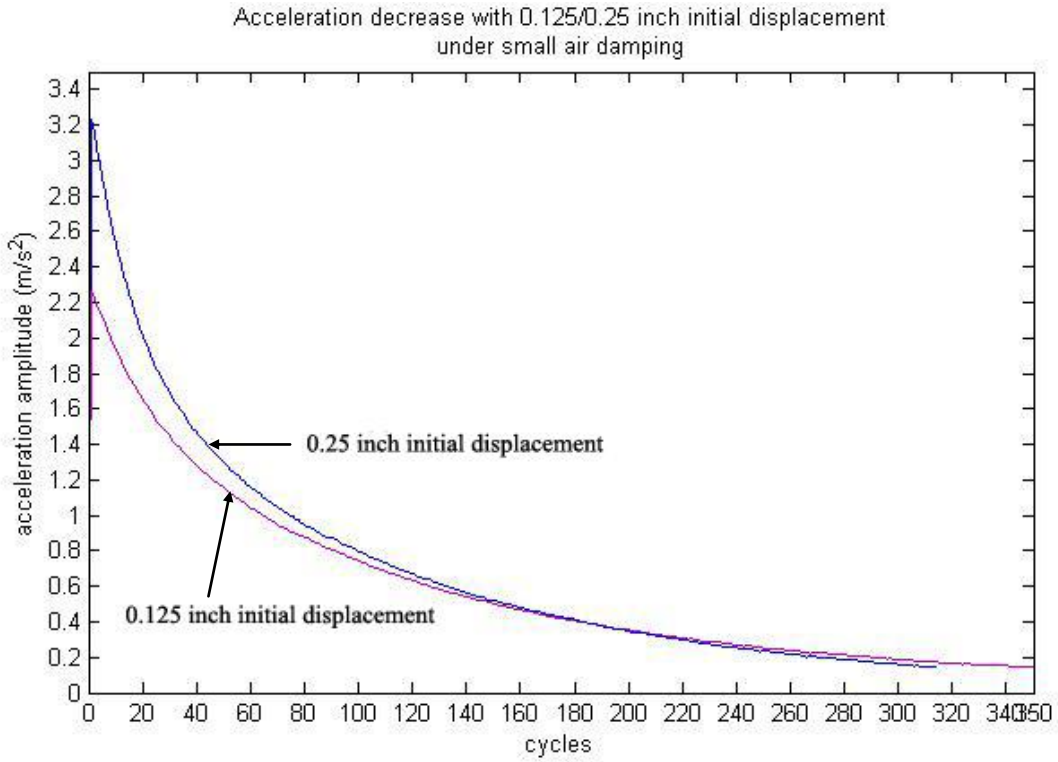

Fig. 7.6 : Acceleration History For Small Air Damping Under both 0.125 Inch And 0.25 Inch Initial Displacement

Fig. 7.5 and Fig. 7.6 show the difference between different initial displacements under the same damping condition. From Fig. 7.5, the large-air damping condition, we observe that for the system to be damped out to the same level, the number of cycles it takes for the 0.25 inch initial displacement case is less than for the 0.125 inch initial displacement case. This means for the same damping condition, a larger initial displacement results in a larger damping effect. Fig. 7.6 shows the same result for the small-air damping condition. Also in Fig. 7.6 (small damping case), we observe that the number of cycles needed for the system to be damped out is more than it is in Fig. 7.5 (large damping case), confirming the damping effect of air.

The damping ratio is calculated based on the experimental acceleration using the equation (approximated but accurate for $\xi \ll 20\%$) given by Chopra [2008]:

$$\xi = \frac{1}{2\pi j} \ln \frac{\ddot{u}_i}{\ddot{u}_{i+j}} \ . \qquad (Eq.\,7.3)$$

where j is the number of cycles. $\ddot{u}_i$ is the acceleration amplitude at cycle i, $\ddot{u}_{i+j}$ is the acceleration amplitude after j cycles. Using Eq. 7.3, the damping ratios for the different cases are calculated.

$\xi_1 = 0.13\%$ for small-air damping with 0.125 inch initial displacement;

$\xi_2 = 0.15\%$ for large-air damping with 0.125 inch initial displacement;

$\xi_1' = 0.16\%$ for small-air damping with 0.25 inch initial displacement;

$\xi_2' = 0.2\%$ for large-air damping with 0.25 inch initial displacement;

Note that these damping ratios are the sum of mechanical damping (internal damping) and air-damping together. Thus, to find the approximate damping effect due to air only, subtract ξ_1 from ξ_2, and subtract ξ_1' from ξ_2'.

As a comparison, the damping ratio based on radiation from an oscillating sphere is calculated using Eq. 4.15, rewritten here.

$$\xi'_{eq1} = \frac{\rho_0 c_0 A}{6\omega m} \frac{(kr_0)^4}{4 + (kr_0)^4} \ . \qquad (Eq.\,4.15)$$

The area of the aluminum plate $A = 1\,ft^2 = 0.093\,m^2$, $r_0 = 0.5\,ft = 0.1524\,m$, $k = \frac{\omega}{c_0}$. Therefore, the equivalent damping ratio can be calculated as:

$$\xi'_{eq1} \cong 1.85 \times 10^{-8}\% \ . \qquad (Eq.\,7.1)$$

The experimental results and theoretical results are shown in Table 7.2.

Damping Ratio for Air	0.125 inch Initial displacement	0.25 inch Initial displacement	Oscillating Sphere
ξ	0.02%	0.04%	$1.85 \times 10^{-8}\%$

Table 7.2 : Damping Ratio for Air Under Different Initial Displacements
Test 1

From Table 7.2 we find that the theoretical damping ratio based on an oscillating sphere is much smaller than test results. We next increase the natural frequency of the system.

7.4 Experimental Setup – Test 2 ($f_2 = 9.56Hz$)

To increase the natural frequency, the length of rods are shortened to $19\ inches$. For this system, the stiffness of a single rod is:

$$k_i = \frac{12EI}{h^3} = \frac{12(29000ksi)(3.974 \times 10^{-4} in^4)}{(19in)^3} = 20.142\frac{lb}{in} = 3527.46\frac{N}{m},$$

The stiffness of the whole system is then:

$$K_2 = 4k_i = 80.568\frac{lb}{in} = 996.816\frac{lb}{ft} = 14109.84\frac{N}{m}.$$

Assume 12 lb of the system is included in the vibration.

$$m_2 = \frac{12\ lb}{32.2\ ft/s^2} = 0.373\ lb \cdot \frac{s^2}{ft} = 5.444\ kg$$

The natural frequency of the system is then found to be:

$$\omega_2 = \sqrt{\frac{K_2}{m_2}} = \sqrt{\frac{996.816\ lb/ft}{0.373\ \frac{lb \cdot s^2}{ft}}} = 51.7\frac{rad}{s}$$

$$f = 51.7\frac{rad}{s} = 8.23\ Hz$$

7.5 Acceleration Measurement and Test Results – Test 2 ($f_2 = 9.56Hz$)

The initial displacements are reduced to 0.125 inch and 0.0625 inch because the increased stiffness has made it difficult to apply a large displacement without yielding the steel rods. Fig. 7.7 and Fig. 7.8 show the test results. The tested natural frequency is 9.56 Hz, which is close to the theoretical natural frequency of 8.23 Hz.

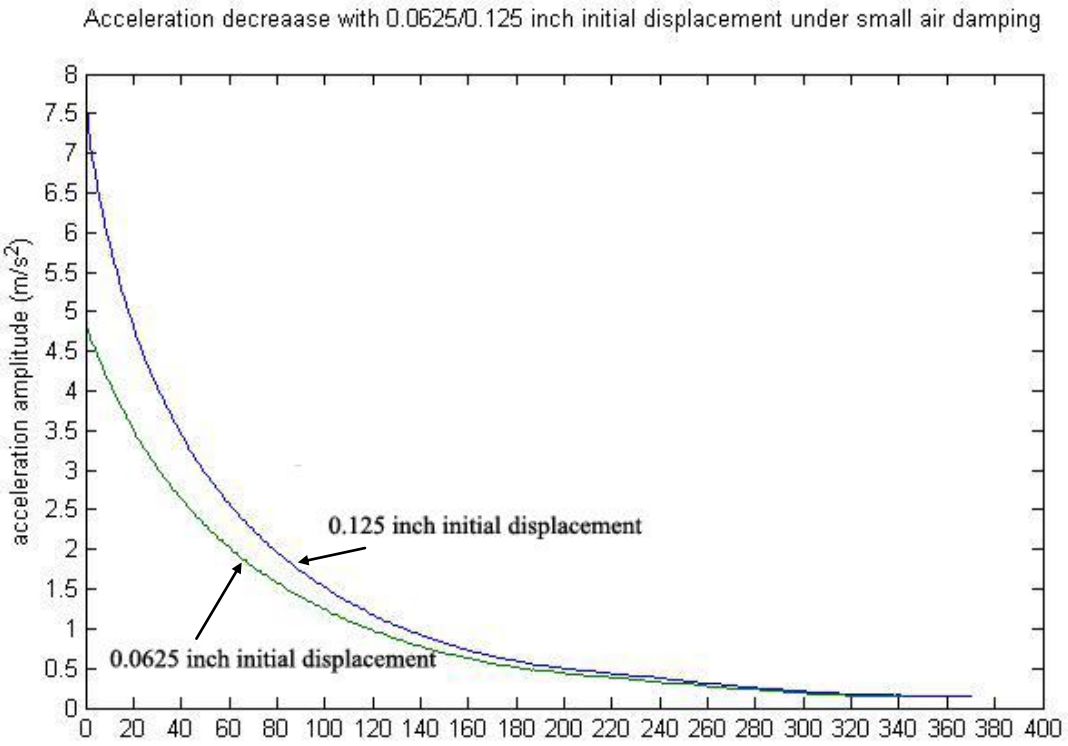

Fig. 7.7 : Acceleration History For Large-Air Damping Under both 0.125 Inch And 0.0625 Inch Initial Displacement

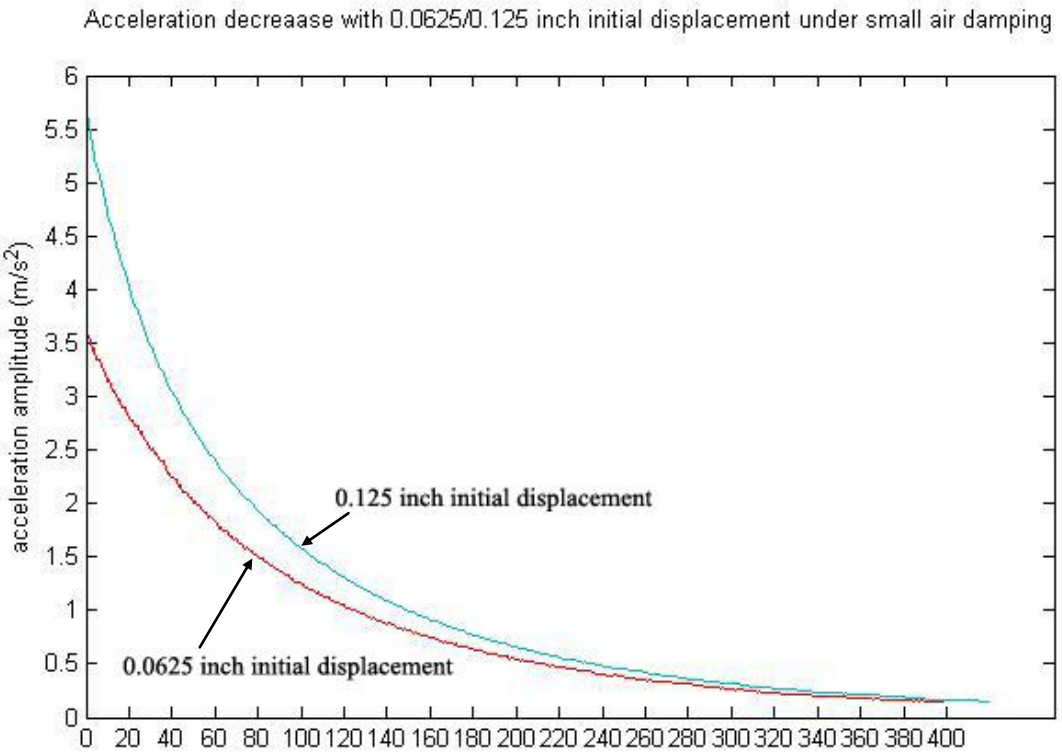

Fig. 7.8 : Acceleration History For Small-Air Damping Under both 0.125 Inch And 0.0625 Inch Initial Displacement

The tested damping ratio is calculated using Eq. 7.3, repeated here:

$$\xi = \frac{1}{2\pi j} \ln \frac{\ddot{u}_i}{\ddot{u}_{i+j}} \ . \qquad (Eq. 7.3)$$

$\xi_1 = 0.14\%$ for small-air damping with 0.125 inch initial displacement;

$\xi_2 = 0.17\%$ for large-air damping with 0.125 inch initial displacement;

$\xi_1' = 0.13\%$ for small-air damping with 0.0625 inch initial displacement;

$\xi_2' = 0.16\%$ for large-air damping with 0.0625 inch initial displacement;

Note that these damping ratios are the sum of mechanical damping (internal damping) and air-damping together. Thus, to find the damping effect of air only, subtract ξ_1 from ξ_2, and subtract ξ_1' from ξ_2'.

Again, the equivalent damping coefficients of air based on radiation from an oscillating sphere is calculated using Eq. 4.15.

$$\xi'_{eq2} \cong 6.5 \times 10^{-7}\% \ . \qquad (Eq. 7.5)$$

The experimental results and theoretical results are shown in Table 7.3.

Damping Ratio for Air	0.125 inch Initial displacement	0.0625 inch Initial displacement	Oscillating Sphere
ξ	0.03%	0.03%	$6.5 \times 10^{-7}\%$

Table 7.3 : Damping Ratio for Air Under Different Initial Displacements
Test 2

From Table 7.3 we again find that the theoretical damping ratio for air based on an oscillating sphere is much smaller than that obtained from the experimental results, even at the higher frequency.

7.6 Applying Fluid Dynamics Theory

In chapter 5 we have derived the expression for damping ratio of a vibrating plate based on fluid dynamics theory. We are now interested in applying Eq. 5.18 to the vibrating plate experiment to see if the fluid dynamics theory applies.

Given that Eq. 5.18 is:

$$\xi_{eq} = \frac{c_{eq}}{c_{cr}} = \frac{1}{4\pi^3}\frac{C_D A \rho_0 \Delta_0}{m} \quad . \qquad (Eq. 5.18)$$

For the vibrating plate experiment,

$A = 1\ ft^2 = 0.093\ m^2$;

$\rho_0 = 1.204\ kg/m^3$;

$k_1 = 4921.732\ N/m$ and $k_2 = 14109.84\ N/m$ respectively;

$m_1 = 6.355\ kg$ and $m_2 = 5.444\ kg$ respectively;

According to Roberson and Crowe [1975], for a specific rectangular plate with $l/B = 1$, the drag coefficient $C_D = 1.18$.

Let $\Delta_0 = 0.125\ inch = 3.175 \times 10^{-3}\ m$ for both experiments, applying Eq. 5.18, two damping ratios are calculated for two systems with different frequencies, but with the same initial displacement.

$$\xi''_{eq\,1} = \frac{1}{4\pi^3}\frac{(1.18)(0.093\ m^2)\left(1.204\frac{kg}{m^3}\right)(3.175 \times 10^{-3}\ m)}{6.355\ kg}$$

$$= 0.000053\% \ .$$

$$\xi''_{eq\,2} = \frac{1}{16\pi^3}\frac{(1.18)(0.093\ m^2)\left(1.204\frac{kg}{m^3}\right)(3.175 \times 10^{-3}\ m)}{5.444\ kg}$$

$$= 0.000062\% \ .$$

The results show that for frequencies of 4.78 Hz and 9.56 Hz, Eq. 5.18 based on

fluid dynamics theory also gives a much lower theoretical damping ratio than the experimental results. We now wonder if this frequency is too high to apply fluid dynamics theory. For this reason, a pendulum experiment is designed and presented in next chapter. The experiment, consisting of a plastic ball hanging from the ceiling, will help us look into a much lower frequency range.

7.7 Summary

In this chapter we have demonstrated that the theoretical damping ratio based on acoustic radiation from an oscillating sphere does not apply when the frequency is low at around 5 Hz and 10 Hz. For the specific experiment with a natural frequency of 4.78 Hz shown in this chapter, the theoretical damping ratio based on acoustic radiation from an oscillating sphere is calculated as $1.85 \times 10^{-8}\%$, compared with the experimental results of 0.02% and 0.04% for different initial displacements. For the other experiment with a natural frequency of 9.56 Hz, the theoretical damping ratio based on acoustic radiation from an oscillating sphere is calculated as $6.5 \times 10^{-7}\%$, compared with the experimental results of 0.03% for different initial displacements. We have also found that for this experiment, fluid dynamics theory does not apply in the frequency range of 5-10 Hz.

The next chapter presents a pendulum experiment consisting of a rigid sphere oscillating at a much lower frequency. We will study the frequency range in which the damping ratio based on fluid dynamics theory is expected to apply.

CHAPTER 8.

PENDULUM EXPERIMENT

8.1 General

In chapter 7, a vibrating plate experiment was presented. We have discovered that the theoretical damping ratio of this vibrating target based on either acoustic radiation from an oscillating sphere or fluid dynamics theory for a plate does not predict the observed damping due to air. In this chapter, a pendulum experiment is presented. The results of the experiment are compared with Eq. 5.18 to investigate the applicability of fluid dynamics theory under very low frequencies.

8.2 Experimental Setup – Test 1 ($f_1 = 0.205\ Hz$)

A light-weight plastic ball hanging from the ceiling using a fishing-line makes a simple pendulum system. By changing the length of the fishing-line, the vibrational frequency of the pendulum can be adjusted. The system is shown in Fig. 8.1.

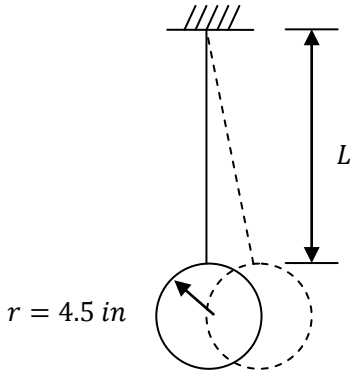

Fig. 8.1: Pendulum System Dimensions

According to literature, the vibrational period of a pendulum is:

$$T = 2\pi\sqrt{\frac{L}{g}}\ . \qquad (Eq.8.1)$$

where g is the acceleration of gravity and $g = 9.8\,m/s^2$. For this experiment, the length of the fishing-line $L_1 = 17.5\,ft = 5.334\,m$. Thus we have

$$T_1 = 2\pi\sqrt{\frac{5.334\,m}{9.8\,\frac{m}{s^2}}} = 4.633\,s\ .$$

The theoretical natural frequency is then:

$$f_1 = \frac{1}{T_1} = \frac{1}{4.633\,s} = 0.216\,Hz\ .$$

An initial horizontal displacement of $5\,ft$ is applied to the pendulum. The plastic ball goes under free vibration after it is released. The horizontal displacements for each cycle are recorded using a tape measure. The damping ratio is calculated for each cycle based on displacement history using the equation given by Chopra [2008]:

$$\xi = \frac{1}{2\pi j}\ln\frac{u_i}{u_{i+j}}\ . \qquad (Eq.8.2)$$

where j is the number of cycles. u_i now is the displacement amplitude at cycle i, u_{i+j} is the displacement amplitude after j cycles.

8.3 Test Results – Test 1 ($f_1 = 0.205\,Hz$)

The actual natural frequency is calculated by using a stopwatch recording the time period for each cycle and averaging all the data recorded. The natural frequency is approximately $0.205\,Hz$, compared to the theoretical natural frequency of $0.216\,Hz$.

A plot of displacement history for the experiment with a natural frequency of $f_1 = 0.205\,Hz$ is shown in Fig. 8.2.

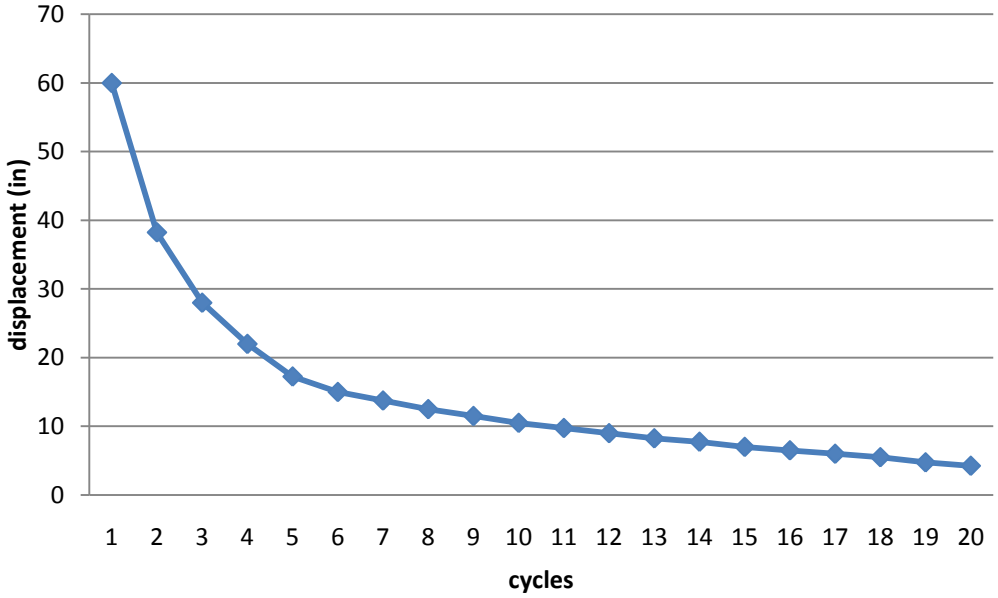

Fig. 8.2: Displacement History of Test 1 ($f_1 = 0.205\ Hz$)

From Fig. 8.2 we can see that the displacement amplitude decreases very rapidly during the first several cycles. Only 20 cycles were recorded because after 20 cycles the decreasing of displacement amplitude for each cycle is hardly distinguishable using the tape measure. The damping ratio for each cycle is calculated using Eq. 8.2. The final damping ratio for the system is calculated by averaging the damping ratios for each cycle. The result is summarized in Table 8.1.

TEST 1	
Theoretical Frequency f	0.216 Hz
Tested Frequency f	0.205 Hz
Tested Damping Ratio ξ	2.22%

Table 8.1: Damping Ratio of Test 1 ($f_1 = 0.205\ Hz$)

8.4 Analytical Solution

In chapter 5 we have shown with Eq. 5.18, the equivalent damping ratio based on fluid dynamics theory is:

$$\xi''_{eq} = \frac{c_{eq}}{c_{cr}} = \frac{1}{4\pi^3}\frac{C_D A \rho_0 \Delta_0}{m} \ . \qquad (Eq. 5.18)$$

where C_D is the coefficient of drag, A is the projected area of the body, ρ_0 is the density of the fluid, Δ_0 is the vibrational amplitude.

The coefficient of drag for a sphere depends on the Reynolds number, which is given as:

$$Re = \frac{VD\rho}{\mu} \ . \qquad (Eq. 8.3)$$

where V is the mean fluid velocity, D is the diameter of the sphere, $D = 9\,in = 0.2286\,m$, ρ is the density of the fluid where the sphere is in, μ is the viscosity of the fluid. For normal atmospheric pressure and a room temperature of 20℃, $\mu = 1.79 \times 10^{-5}\ N \cdot s/m^2$. To find the mean fluid velocity, we take the time-averaged speed of each cycle and calculate the average speed, thus $V = 0.313\ m/s$. Now the Reynolds number is calculated as:

$$Re = \frac{VD\rho}{\mu} = \frac{0.313\frac{m}{s} \times 0.2286\ m \times 1.204\ kg/m^3}{1.79 \times 10^{-5}\ N \cdot s/m^2} = 4812.75$$

According to Hemmati [2009], the coefficient of drag for a sphere is given as:

$$C_D \approx \frac{24}{Re} + \frac{6}{1+\sqrt{Re}} + 0.4 \ . \qquad (Eq. 8.4)$$

For $Re = 4812.75$, the coefficient of drag is:

$$C_D \approx \frac{24}{4812.75} + \frac{6}{1+\sqrt{4812.75}} + 0.4 \approx 0.5 \ .$$

Substituting $C_D = 0.5$ into Eq. 5.18, the damping ratio for a vibrating sphere based on drag is:

$$\xi''_{eq} = \frac{1}{4\pi^3}\frac{(0.5)A\rho_0\Delta_0}{m} = 0.004\frac{A\rho_0\Delta_0}{m} \ . \qquad (Eq. 8.5)$$

The damping ratio for each cycle is thus calculated using Eq. 8.5 and averaged. Substituting the weight of the rubber ball, $m = 9.146 \times 10^{-3} kg$; the density of air

$\rho_0 = 1.204\ kg/m^3$; the projected area of the ball $A = 0.041\ m^2$, and displacement amplitudes for each cycle into Eq. 8.5, the averaged equivalent damping ratio is

$$\xi''_{eq1} \cong 1\% \ .$$

The theoretical damping ratio is of the right order of magnitude, which is close to the experimental result, which is $\xi_{eq} = 2.22\%$. A difference exists because for the first several cycles of vibration, the displacements are too large for the sphere to be considered as a transversely oscillating sphere.

8.5 Experimental Setup – Test 2 ($f_2 = 0.265\ Hz$)

By shortening the length of the line from $17.5\ ft$ to $10.75\ ft = 3.277\ m$, the natural frequency of the pendulum can be adjusted. The same process to calculate the theoretical natural frequency can be performed as in section 8.2.

The vibration period of the pendulum is calculated as:

$$T_2 = 2\pi\sqrt{\frac{3.277\ m}{9.8\ \frac{m}{s^2}}} = 3.631\ s \ .$$

The natural frequency is then:

$$f_2 = \frac{1}{T_2} = \frac{1}{3.631\ s} = 0.275\ Hz \ .$$

8.6 Test Results – Test 2 ($f_2 = 0.265\ Hz$)

The actual natural frequency is calculated by using a stopwatch recording the time period for each cycle and averaging all the data recorded. The natural frequency is approximately $0.265\ Hz$, compared to the theoretical natural frequency of $0.275\ Hz$.

A plot of displacement history for the experiment with a natural frequency of $f_1 = 0.265\ Hz$ is shown in Fig. 8.3.

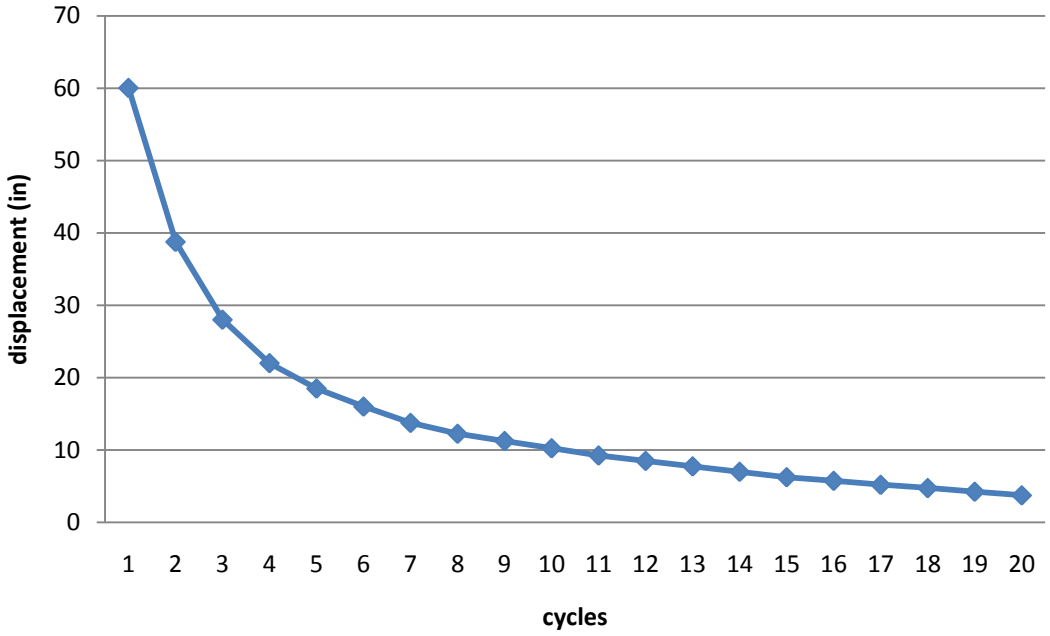

Fig. 8.3: Displacement History of Test 1 ($f_2 = 0.265\ Hz$)

The damping ratio for each cycle is calculated using Eq. 8.2. The final damping ratio for the system is calculated by averaging the damping ratios for each cycle. The result is shown in Table 8.2.

TEST 2	
Theoretical Frequency f	0.275 Hz
Tested Frequency f	0.265 Hz
Tested Damping Ratio ξ	2.32%

Table 8.2: Damping Ratio of Test 2 ($f_2 = 0.265\ Hz$)

8.7 Analytical Solution

Given the damping ratio for a vibrating plate based on drag is:

$$\xi''_{eq} = 0.004\frac{A_p \rho \Delta_0}{m} \ . \qquad (Eq. 8.5)$$

The damping ratio for each cycle is thus calculated using Eq. 8.5 and averaged. Again, substituting $m = 9.146 \times 10^{-3} kg$, $\rho = 1.204\ kg/m^3$, $A_p = 0.041\ m^2$ and

displacement amplitudes for each cycle into Eq. 8.5, the averaged equivalent damping ratio is

$$\xi''_{eq2} \cong 1\ \% \ .$$

The theoretical damping ratio is of the same order of magnitude as experimental result, which is $\xi_{eq} = 2.15\%$.

8.8 Damping Ratio Based on Acoustic Radiation from an Oscillating Sphere

In chapter 4, Eq. 4.15 gives the solution to the equivalent damping ratio based on acoustic radiation from an oscillating sphere.

$$\xi'_{eq} = \frac{\rho_0 c_0 A}{6\omega m} \frac{(kr_0)^4}{4 + (kr_0)^4} \ . \qquad (Eq.4.15)$$

To study the applicability of Eq. 4.15 under low frequency, we apply Eq. 4.15 to the pendulum experiment. Substituting the weight of the rubber ball, $m = 9.146 \times 10^{-3} kg$; the density of air $\rho = 1.204\ kg/m^3$; the projective area of the ball $A_p = 0.041\ m^2$, the speed of sound $c_0 = 340\ m/s$, and the vibrational frequencies $f_1 = 0.205\ Hz$ and $f_2 = 0.265\ Hz$ into Eq. 4.15, we obtain the equivalent damping ratios based on acoustic radiation from an oscillating sphere:

$$\xi'_{eq1} = \frac{\left(1.204 \frac{kg}{m^3}\right)\left(340 \frac{m}{s}\right)(0.041\ m^2)}{12\pi(9.146 \times 10^{-3} kg)(0.205\ Hz)} \frac{(0.00043)^4}{4 + (0.00043)^4} \cong 6.2 \times 10^{-10}\ \% \ ,$$

$$\xi'_{eq2} = \frac{\left(1.204 \frac{kg}{m^3}\right)\left(340 \frac{m}{s}\right)(0.041\ m^2)}{12\pi(9.146 \times 10^{-3} kg)(0.265\ Hz)} \frac{(0.00056)^4}{4 + (0.00056)^4} \cong 3.4\ \times 10^{-9}\% \ .$$

The results based on radiation from an oscillating sphere totally disagree with experimental results. This is expected since the frequency is too low for Eq. 4.15 to be applicable.

8.9 Experimental Result Analysis

Table 8.3 summarizes the results of two experiments together.

	TEST 1	**TEST 2**
Theoretical f	0.216 Hz	0.275 Hz
Tested f	0.205 Hz	0.265 Hz
Theoretical ξ_{eq} (Fluid Dynamics)	1%	1%
Theoretical ξ_{eq} (Oscillating Sphere)	$6.2 \times 10^{-10}\%$	$3.4 \times 10^{-9}\%$
Tested ξ_{eq}	2.22%	2.32%

Table 8.3: Comparison between Test 1 and Test 2

From Table 8.3, we see that the fluid dynamics theory gives a reasonable solution for the damping ratio at frequencies of less than 1 Hz. Some approximations and assumptions should be noted:

1. We have assumed the swinging motion of the pendulum is the same as that of a transversely oscillating sphere. This assumption works only when the rotation angle is small enough to be neglected. For the two experiments performed above, even large rotation angles were taken into account in the calculations.
2. An approximation is that we have used the time-averaged speed in Eq. 8.3 when obtaining the Reynolds number. However according to Roberson and Crowe [1975], using the actual speed function will not lead to a big difference in the coefficient of drag, because the coefficient of drag stays approximately at the same value with regard to a large range of Reynolds Number.

Through the vibration plate experiment and the pendulum experiment, we have studied the applicability of acoustic theory based on acoustic radiation from an oscillating sphere and fluid dynamics theory at two frequency ranges. The experimental results show that the acoustic theory does not apply for low frequency vibrations. We believe that the acoustic theory is only valid for high-frequency vibrations. The fluid dynamics theory applies reasonably well for low frequency range that we used in the pendulum experiment.

In the next chapter a baffled plate experiment will be presented, testing the applicability of acoustic theory at higher frequency.

CHAPTER 9.

BAFFLED PISTON EXPERIMENT

9.1 General

We have performed an unbaffled oscillating plate experiment and a pendulum (oscillating sphere) experiment to determine the applicability of acoustic theory and fluid dynamics theory under various frequency ranges. In chapter 7, based on the oscillating plate experiment, we showed that neither acoustic theory based on radiation from an oscillating sphere nor fluid dynamics theory accurately predicts the energy loss from a vibrating plate with a frequency range from 5 Hz to10 Hz. We expect that acoustic theory based on acoustic radiation from an oscillating sphere may work at high vibrational frequencies. However, at high frequencies, it would be difficult to keep the plate rigid. In chapter 8 we showed that fluid dynamics theory reasonably predicts the energy loss from a vibrating pendulum with a frequency of around 0.2 Hz.

In this chapter, to study the applicability of acoustic theory at higher frequencies, a baffled piston experiment is described. As stated in chapter 6, a baffled piston is an infinite plane (the baffle) except for a section (the piston) that vibrates normal to the surface. We have derived the theoretical solution for the acoustic field produced by the vibration of a baffled piston using the Rayleigh Integral (Blackstock [2000]). In this chapter, a vibrating plate experiment is designed to act like a baffled piston. Experimental results are compared with the theoretical Rayleigh Integral solution to verify the applicability of acoustic theory at high frequency.

9.2 Experimental Setup

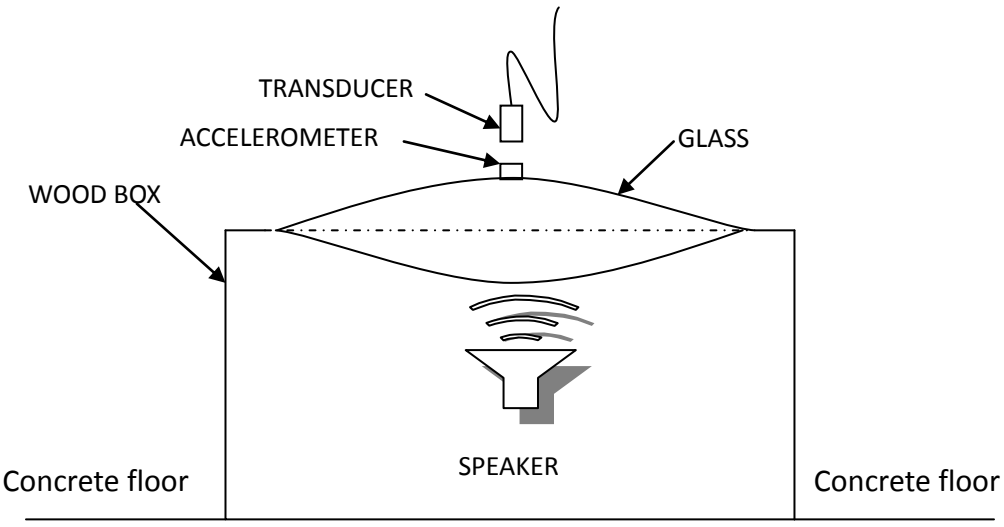

Fig. 9.1: Sketch of Experimental Setup

A plate of glass is fixed to a wood box, as shown in Fig. 9.1. The wood box with one face open is used to act as a rigid baffle. Note this is an approximation because the wood box is not an infinite plane. The glass plate is mounted using aluminum strips on the edges of the open face of the box.

A speaker placed inside the wood box generates harmonic excitations. The frequencies generated by the speaker are controlled by Matlab. Different vibrational modes of the glass are excited by various harmonic frequencies. For example, Fig. 9.1 shows the first vibrational mode of the glass. At this mode the glass vibrates up and down as shown. An accelerometer attached to the glass collects acceleration data. An acoustic pressure transducer is placed at various distances from the glass to acquire pressure data. Styrofoam pieces with thickness of 0.5 inch are placed inside of the box to damp out vibrations of the sides of the box.

The speaker is a Boston Acoustics® BA265™ Speaker. The diameter is 3 in,

with an output power of 92 decibels and frequency response in the range of 100 to 20,000 Hertz. The Matlab code that controls the speaker was written by Ortega [2008] and is shown in Fig. 9.2.

```
function input_file = inputs
%
%
%This program generates the vector of the sound variation. Also plays
this
%sound vector at any desired frequencies and with any desired
duration.
%
%Input Frequency Range
freqs = [151:1:155];
n_freq = size(freqs,2);
p_time = 10;%%Time in seconds the sound is going to be played
n_cyc_req = p_time*freqs;
%Generate the required number of cycles of Sinusoidal Excitation
steps_per_cycle = 100;
y_s = zeros(n_freq,(n_cyc_req(1,n_freq))*steps_per_cycle + 1);
T =   zeros(n_freq,(n_cyc_req(1,n_freq))*steps_per_cycle + 1);
sample_step = 2*pi/steps_per_cycle;
for i = 1:n_freq
    cn = 0;
    for t = 0:sample_step:2*pi*n_cyc_req(1,i)
        cn = cn + 1;
        y_s(i,cn) = sin(t);
        T(i,cn) = t;
    end
end
for j = 1:n_freq
Fs = freqs(1,j)*steps_per_cycle;
y = y_s(j,1:n_cyc_req(1,j)*steps_per_cycle + 1);
wavplay(y,Fs)
end
return
```

Fig. 9.2: Matlab Code For Speaker Control

Fig. 9.3 shows a photograph of the experiment.

Fig. 9.3: Photo of Experimental Devices

The properties of the wood box and glass are shown in Fig. 9.4(a) and Fig. 9.4(b). The plywood has a thickness of 0.5 inch. All edges of the box are framed with $2\ in \times 2\ in$ and $2\ in \times 4\ in$ dimension lumber.

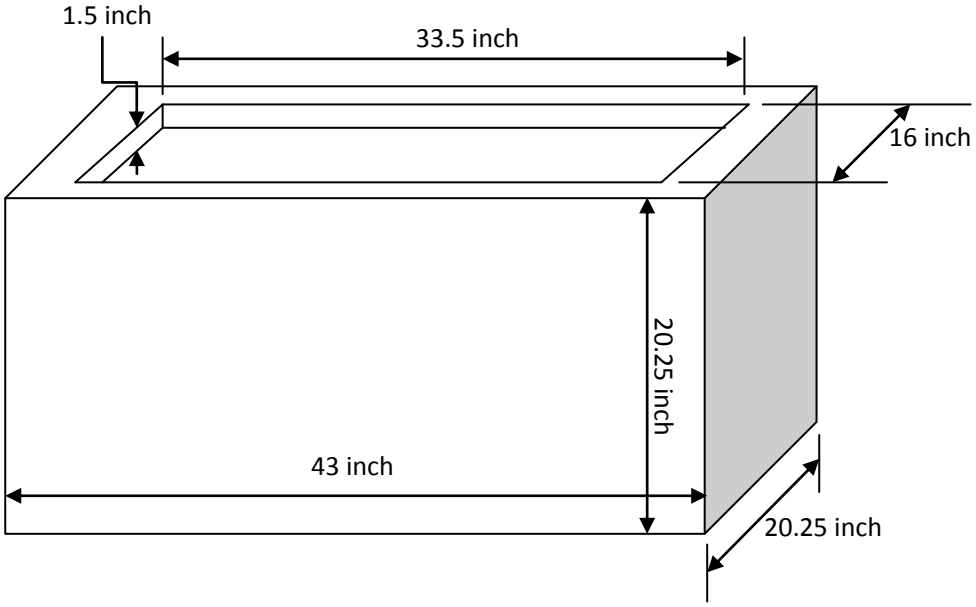

(a): Box and Hole Dimensions

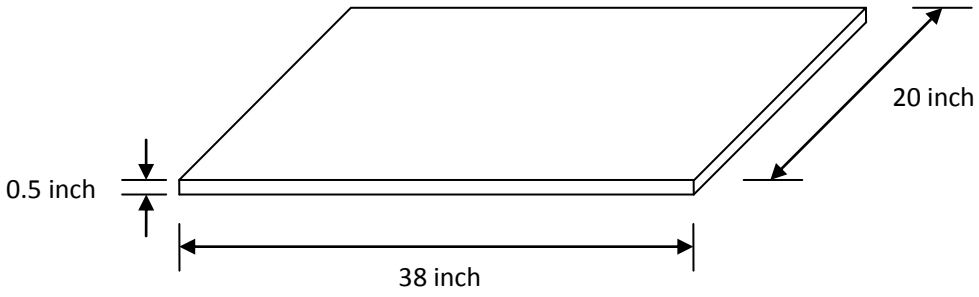

(b): Glass Dimensions

Fig. 9.4: Experimental Setup and Device Dimensions

The physical properties of the glass are obtained from the literature as:

Young's Modulus of glass: $E = 70\ GPa$,

Density of glass: $\rho = 2500\ kg/m^3$

Poisson's Ratio of glass: $\nu = 0.17$

9.3 Finite Element Modeling

The finite element software SAP 2000 is used to compute the modal behavior of the glass plate. The plate is assumed to be clamped at all edges. A modal analysis is completed in SAP 2000 and a series of harmonic frequencies is calculated. The corresponding mode shapes are also generated. The first two modes' natural frequencies are given in Fig. 9.5(a) and Fig. 9.5(b), which are 301.67 Hz for the first mode and 400.66 Hz for the second mode.

The results generated from the finite element software will be compared with the experimental results to verify the natural frequencies of the glass. Fig. 9.5 also shows the mode shapes generated by SAP 2000.

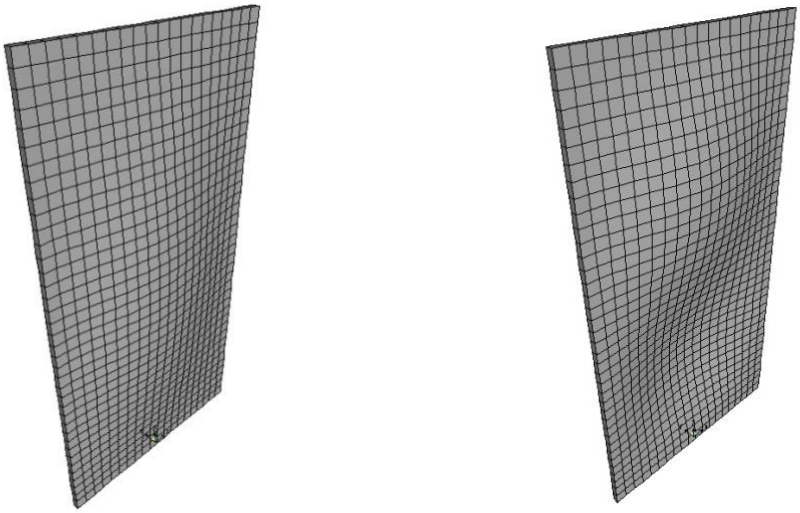

(a) First Mode (301.67 Hz) **(b) Second Mode (400.66 Hz)**

Fig. 9.5 Mode Shapes and Natural Frequencies from SAP 2000

9.4 Experimental Result (Acceleration)

To verify the finite element results, the acceleration response history from the attached accelerometer under various driving frequencies is plotted in Fig. 9.6. The driving frequencies are increased from 50 Hz to 450 Hz, with a step of 1 Hz. The acceleration data is acquired from a data acquisition toolbox using the software Labview. The frequency response is recorded and processed using Microsoft Excel.

The acceleration response history in Fig. 9.6 shows that there are two major peaks where the acceleration amplitude is high and distinguishable. These are the acceleration peaks at the harmonic frequencies of the glass. They are at 299 Hz and 393 Hz, respectively.

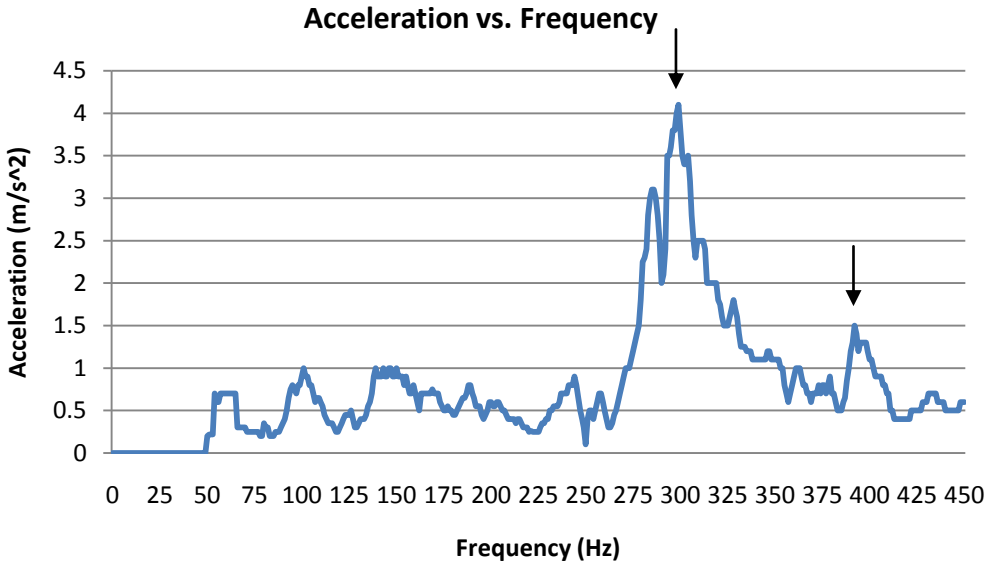

Fig. 9.6: Acceleration Response History vs. Driving Frequencies

Note that in Fig. 9.6 we can see some minor peaks exist. These peaks could be due to vibrational modes of the wood box.

A comparison of computer modeling and experimental results are shown in Table 9.1:

	Modeling Result (Hz)	Experiment Result (Hz)
Mode 1	301.67	299
Mode 2	400.66	393

Table 9.1: Computer and Experimental Result Comparison

We can see that minor differences exist. For example in the second mode, the experiment result (393 Hz) has a difference of 7 Hz compared to the computer modeling result (400.66 Hz). This could be due to the imperfect modeling of boundary conditions. However we are interested only in the first mode because its mode shape is closer to a uniformly vibrating baffled piston.

From the acceleration response history we can see the finite element software SAP 2000 has successfully calculated the natural frequencies of the glass. Now we are interested in the acoustic field when the glass is vibrating in its first mode.

9.5 Experimental Result (Pressure)

In chapter 6 we derived Eq. 6.30 for the farfield pressure along the central axis normal to the baffled piston surface. To verify the equation, the acoustic pressure transducer is placed pointing toward the center of the glass, at various distances above the center of the glass plate. The distance is increased from 1 inch to 60 inches with a step of 1 inch. The speaker driving frequency is fixed at 299 Hz, which is the frequency of the 1st vibrational mode of the glass. For each distance step, pressure data is collected and processed to acquire an average peak value. The pressure amplitude is plotted versus distance in Fig. 9.7.

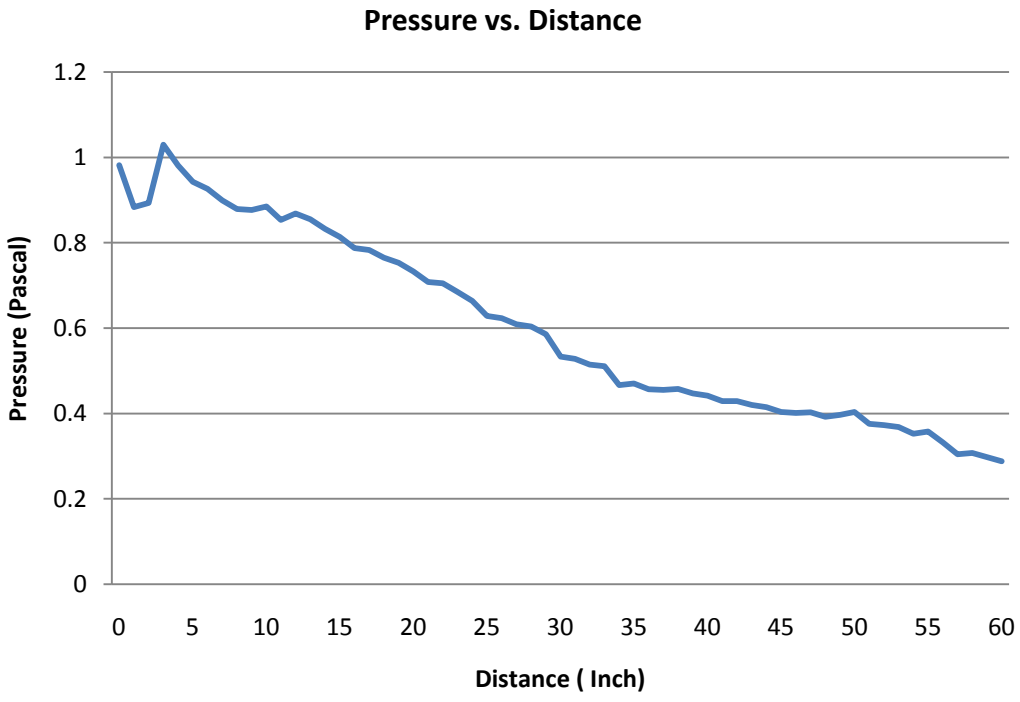

Fig. 9.7: Pressure Amplitude vs. Distance

From Fig. 9.7, we see that at a distance of 3 inches, the pressure amplitude reaches its peak value of 1.0293 Pascal. Then it decreases with increasing distance.

9.5.1 Theoretical Pressure Based on Experimental Devices

Eq. 6.30 gives the expression for farfield pressure amplitude along the central axis normal to the baffled piston surface, rewritten here:

$$p = \frac{P_0 R_0}{r} . \qquad (Eq. 6.30)$$

where the Rayleigh distance R_0 is defined by the ratio of the piston area to the wave length:

$$R_0 = \frac{S}{\lambda} , \qquad (Eq. 9.1)$$

and P_0 is defined as:

$$P_0 = \rho_0 c_0 u_0 . \qquad (Eq. 9.2)$$

where ρ_0 is the density of air, c_0 is the speed of sound in the same air media. u_0 is the vibrational speed amplitude of the piston.

To evaluate the theoretical value for the experiment, let us take the properties of air and the glass in to the expression, with $\rho_0 = 1.204\ kg/m^3$ and $c_0 = 340\ m/s$.

To calculate the vibrational speed amplitude, u , the peak acceleration amplitude is read from the acceleration data, which is $4.1\ \mathrm{m/s^2}$. The acceleration, $\dot{u}$, is expressed as a cosine function:

$$\dot{u} = \dot{u_0} \cos \omega t$$

Integrating the acceleration over *t*, we get the expression for velocity, u:

$$u = \int \dot{u} dt = \frac{\dot{u_0}}{\omega} \sin \omega t .$$

The amplitude of the velocity is:

$$u_0 = \frac{4.1 m/s^2}{\omega} = \frac{4.1 m/s^2}{2\pi \times 299\ Hz} = 0.00218 \frac{m}{s}.$$

For the rectangular glass plate, the Rayleigh distance is:

$$R_0 = \frac{S}{\lambda} = \frac{bh}{\lambda}\ .$$

The wave length is:

$$\lambda = \frac{c_0}{f} = \frac{340\ m/s}{299\ Hz} = 1.137\ m\ .$$

Substituting

$$b = 20\ inch = 0.508\ m\ ,$$

$$h = 38\ inch = 0.965\ m\ ,$$

the Rayleigh distance is calculated as:

$$R_0 = \frac{bh}{\lambda} = \frac{0.508m \times 0.965m}{1.137\ m} = 0.4312\ m = 16.97\ in\ .$$

P_0 is calculated as:

$$P_0 = \rho_0 c_0 u_0 = 1.204 \frac{kg}{m^3} \times 340 \frac{m}{s} \times 0.00218 \frac{m}{s} = 0.8924 \frac{kg}{m \times s^2}\ ,$$

or:

$$P_0 = 0.8924 \frac{kg}{m \times s^2} = 0.8924 \frac{N}{m^2} = 0.8924\ Pa\ .$$

The expression of pressure amplitude at different distances from the plate surface is then:

$$p = \frac{P_0 R_0}{r} = \frac{0.8924\ Pa \times 16.97\ in}{r} = \frac{15.14}{r}\ (Pa) \qquad (Eq.\ 9.3)$$

9.6 Comparison of Experiment and Theory

Based on Eq. 9.3, theoretical pressure p is plotted against various distances r $(1 - 60\ inch)$ in Fig. 9.8. The experiment result is also plotted in the same figure.

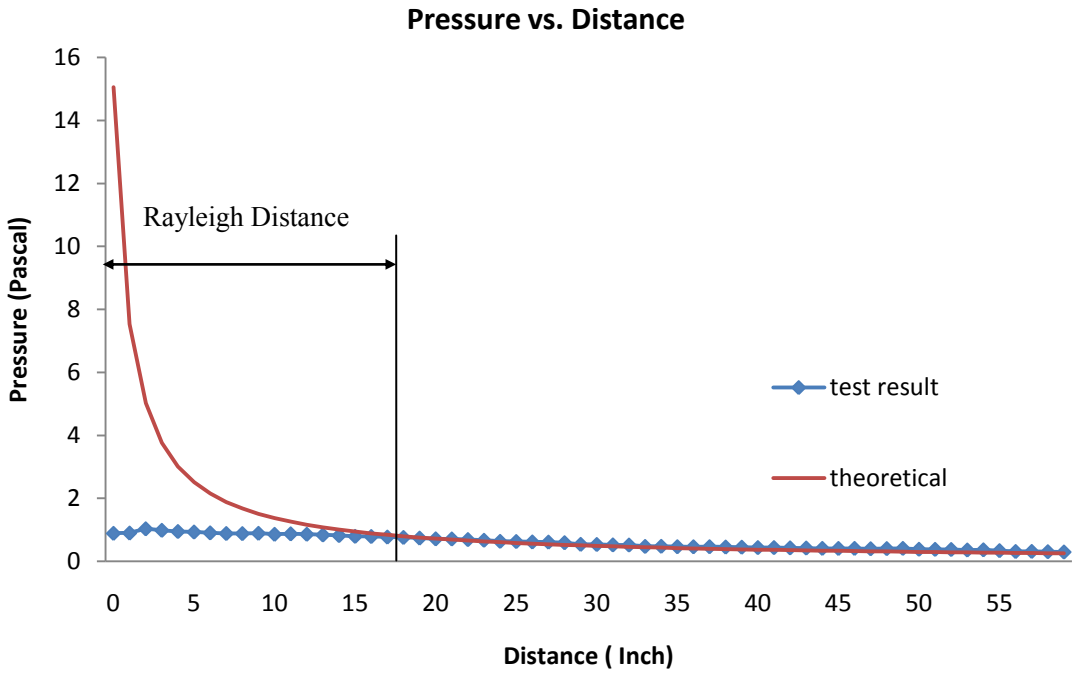

Fig. 9.8: Theoretical and Experimental Results Comparison

9.6.1 Farfield Pressure

From Fig. 9.8, theoretical pressure amplitude doesn't match with test pressure amplitude until the field point is approximately 17 inches away from the glass surface. After the distance of 17 inch, the two matches each other closely. According to the calculation, the Rayleigh Distance $R_0 = 16.97\ in$, this result is close to the distance (around 17 inch) at which the farfield theoretical pressure and experimental pressure match each other.

Blackstock [2000] suggests in his book *Fundamentals of Physical Acoustics* that the Rayleigh Distance R_0 can be loosely interpreted as the cutoff distance between nearfield and farfield. This means the piston radiation starts out as a collimated plane wave form. Beyond the distance of $R_0 = 16.97\ in$, the wave spreads spherically. This idea is shown in Fig. 9.9.

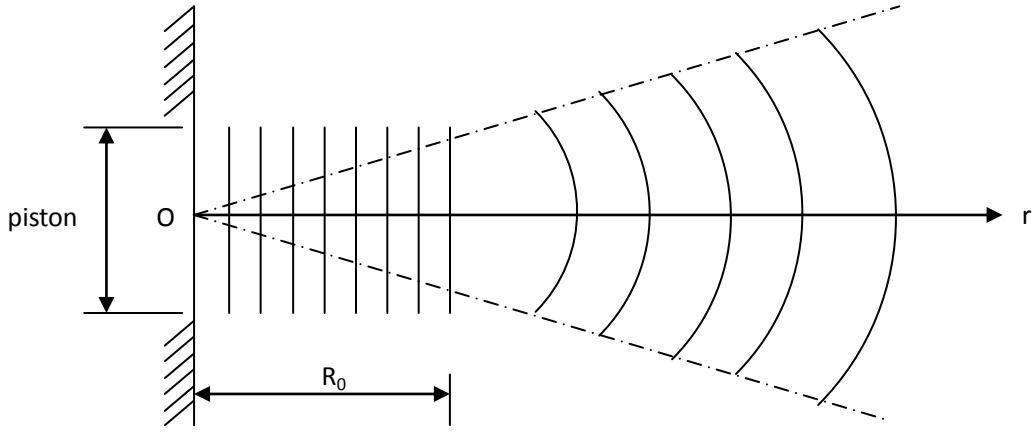

Fig. 9.9: Geometrical demonstration of Rayleigh Distance and wave shape

The result matches our expectation because the Rayleigh Integral solution, Eq. 9.3 gives only the farfield solution along the central axis normal to the piston surface. Thus, it is not surprising that the theoretical pressure in Fig. 9.8 doesn't match with test result until the distance exceeds the Rayleigh Distance R_0. Then what is the theoretical pressure in the nearfield?

9.6.2 Nearfield Pressure

Blackstock [2000] suggests that the nearfield pressure on the central axis normal to the piston can be calculated using the following equation:

$$p = j2P_0 \sin\left[\left(\frac{k}{2}\right)\left(\sqrt{r^2 + a^2} - r\right)\right] e^{j(\omega t - kr - \xi)} . \qquad (Eq. 9.4)$$

where ξ is defined as:

$$\xi = k(\sqrt{r^2 + a^2} - r)$$

However, since $e^{j(\omega t - kr - \xi)}$ is basically a sine function, we can focus on the amplitude of the pressure. That is,

$$p' = 2P_0 \sin\left[\left(\frac{k}{2}\right)\left(\sqrt{r^2 + a^2} - r\right)\right] . \qquad (Eq. 9.5)$$

where some of the variables have been calculated previously:

$$P_0 = \rho_0 c_0 u_0 = 0.8924 \frac{kg}{m \times s^2} \ ,$$

and

$$k = \frac{\omega}{c} = \frac{2\pi f}{c} = \frac{6.28 \times 299\ Hz}{340\ m/s} = 5.52\ \frac{1}{m} \ .$$

In Eq. 9.5, the amplitude of nearfield pressure p' is then a function of distance r, which is the distance from the piston surface to the field point on central axis. Note the limit of r is that $r < R_0 = 16.97\ inch$ for nearfield analysis. A figure of theoretical nearfield pressure is plotted in Fig. 9.10.

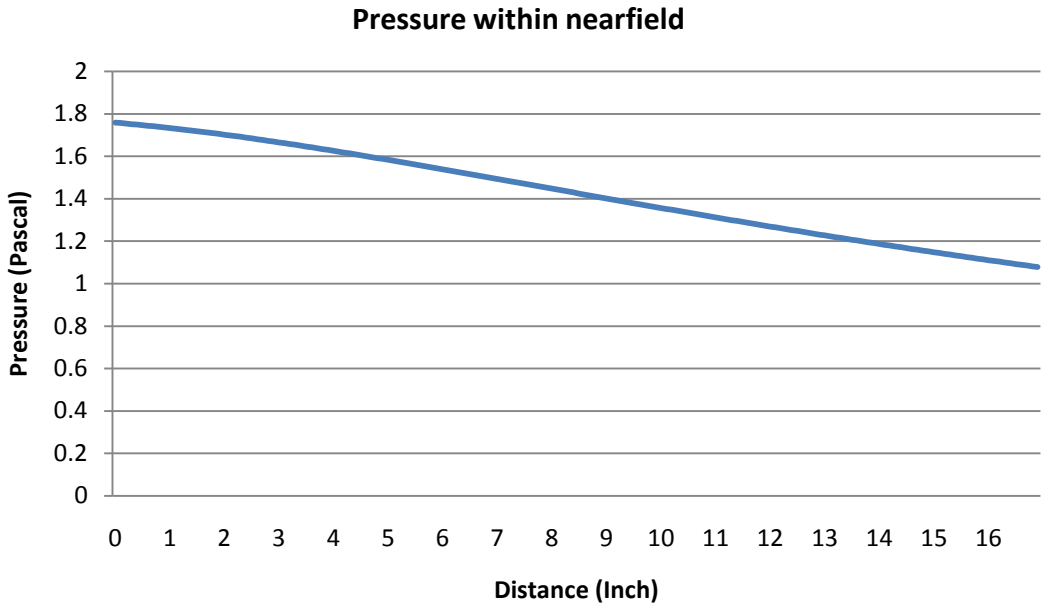

Fig. 9.10: Theoretical nearfield amplitude along the central axis

In Fig. 9.10, the distance r varies from 0 to 17 inch, which is within the range of the Rayleigh distance. Fig. 9.10 shows a smooth decrease of pressure amplitude within the nearfield.

9.6.3 Combination of Nearfield and Farfield Pressures

Finally, let us combine the theoretical pressure of both nearfield and farfield, then compare the theoretical predictions with the test result. The comparison is plotted

in Fig. 9.12.

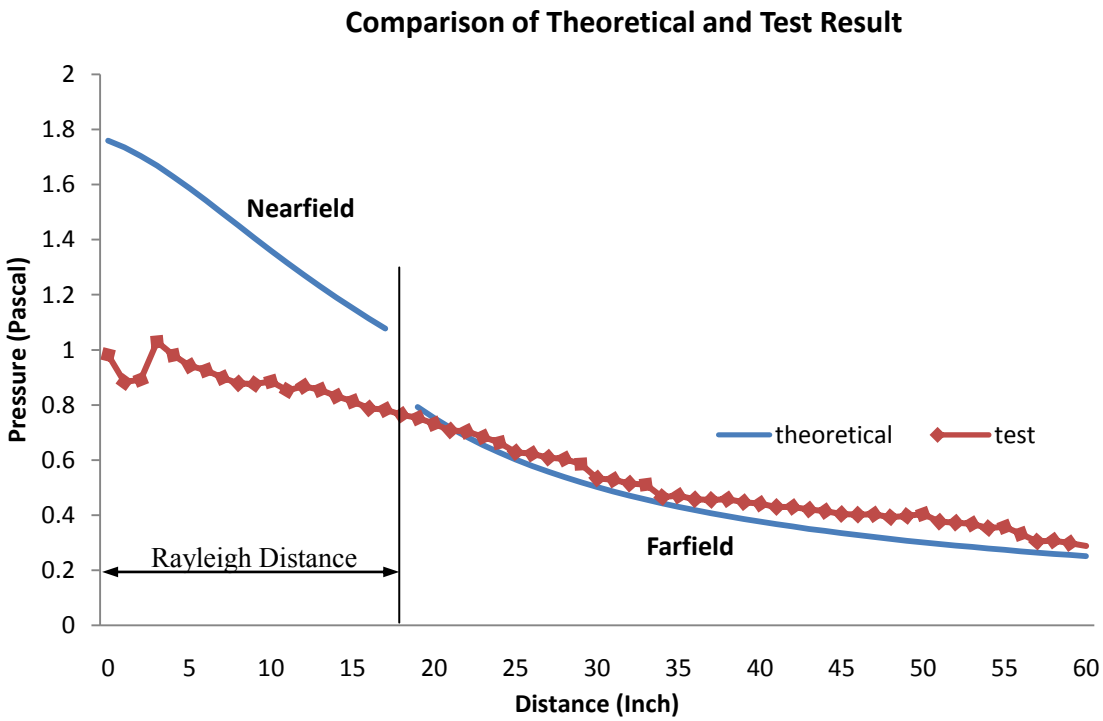

Fig. 9.12: Final Result Comparison

From Fig. 9.12, we see that within Rayleigh distance, theoretical nearfield pressure value is greater than the test result. Once the distance gets into farfield, the theoretical farfield pressure shows a better match with the test result.

9.7 Discussion

In conclusion, the test result matches with the theoretical result as closely as can be expected. Some differences appear in the nearfield. The differences can be explained as follows:

(a) The theoretical nearfield solution assumes the piston is oscillating as a rigid body. However within the Rayleigh distance, when the pressure transducer is relatively close to the vibrating glass, the glass is apparently vibrating non-uniformly because the boundaries are fixed to the wood box. This means the

effective piston size is smaller than what we used in nearfield pressure calculation. If we substitute a dimension smaller than the actual glass size into the numerical study, we could find that the nearfield curve gets somewhat closer to the test result. This result is plotted in Fig. 9.13.

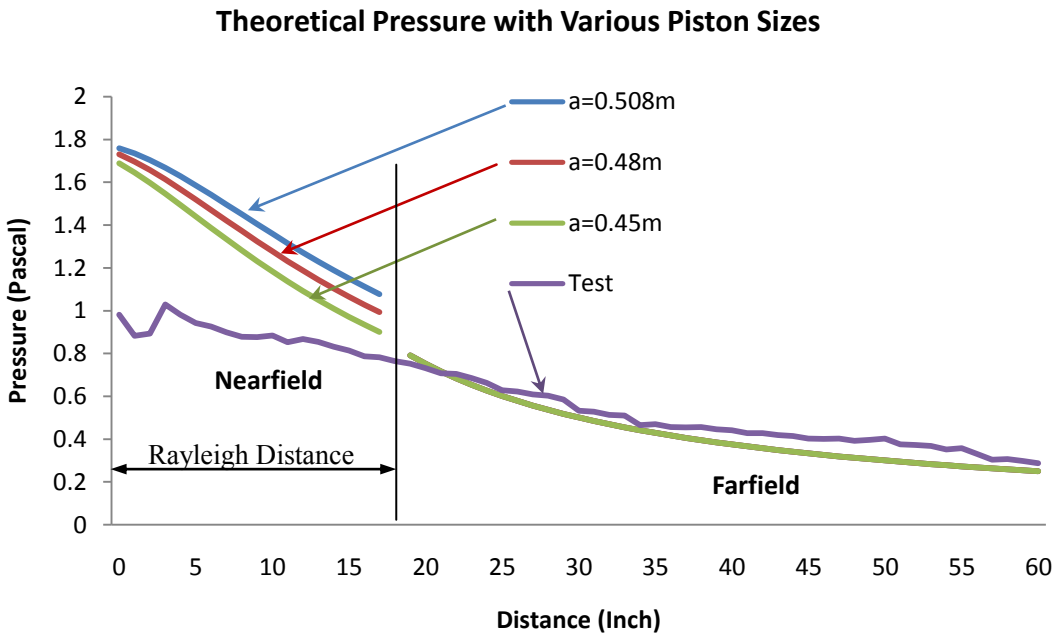

Fig. 9.13: Theoretical pressure with various piston sizes vs. test result

From Fig. 9.13, within nearfield, we see when a piston with radius of 0.45 m is assumed, the nearfield and farfield pressure shows a smoother transition. This is 2.28 inches smaller in radius than what we used for theoretical nearfield pressure calculation. However, there still exists a difference between the theoretical result and experimental result.

(b) As stated earlier, the geometry of the wood box does not satisfy the ideal assumption of a baffle, which is an infinite plane.

(c) Other reasons may include environmental effects such as noise during the

experiment and so on.

9.8 Theoretical Damping Ratio

The baffled piston's behavior can be modeled as one-half of a pulsating sphere. Thus the expression for the damping ratio based on radiation from a pulsating sphere can be used to calculate the theoretical damping ratio. In chapter 4, we derived the expressions for equivalent damping ratios based on acoustic radiation from a pulsating sphere, repeated here:

$$\xi_{eq} = \frac{\rho_0 c_0 A}{2\omega m} \frac{(kr_0)^2}{1+(kr_0)^2} \ . \qquad (Eq.\,9.6)$$

For the baffled plate experiment,

$\rho_0 = 1.204\ \frac{kg}{m^3}$,

$c_0 = 340 \frac{m}{s}$,

$A = 0.508m \times 0.965m = 0.49\ m^2$,

$m = 15.6\ kg$,

$\omega = 2\pi f = 2\pi(299\ Hz) = 1877.72 \frac{rad}{s}$,

$kr_0 = \left(5.52\ \frac{1}{m}\right)(0.508\ m) = 2.8$.

Thus, the theoretical damping ratio due to acoustic radiation for a rigid vibrating glass plate is:

$$\xi_{eq} = \frac{\left(1.204\ \frac{kg}{m^3}\right)\left(340 \frac{m}{s}\right)(0.49\ m^2)}{2\left(1877.72 \frac{rad}{s}\right)(15.6\ kg)} \frac{(2.8)^2}{1+(2.8)^2} \cong 0.3\% \ .$$

This theoretical result seems reasonable. Unfortunately, because of the weight and size of the glass plate, it is very difficult to use the glass plate to make a rigid vibrating system at high frequency. The data processing capacity requirement for a

computer will also be much higher.

We have shown that the Rayleigh Integral works well to predict the acoustic pressure caused by the baffled piston at a frequency of around 300 Hz. Thus the damping ratio would be expected to be reasonably well predicted. The next chapter presents analysis and discussion of all the experiments.

CHAPTER 10.

ANALYSIS AND DISCUSSION

10.1 Theoretical Equations and Test Results

In chapter 4, we derived the expressions for equivalent damping ratios based on acoustic radiation from a pulsating sphere and an oscillating sphere. In chapter 5, we derived the expression for equivalent damping ratio of an oscillating rigid plate based on fluid dynamics theory. In chapter 6, we derived the Rayleigh Integral which solves for the farfield pressure of a baffled piston, which is identical to the problem of a pulsating sphere. All these equations are rewritten here for comparison.

The damping ratio based on acoustic radiation from a pulsating sphere is:

$$\xi_{eq} = \frac{\rho_0 c_0 A}{2\omega m} \frac{(kr_0)^2}{1+(kr_0)^2} \ . \qquad (Eq.10.1)$$

The damping ratio based on acoustic radiation from an oscillating sphere is:

$$\xi'_{eq} = \frac{\rho_0 c_0 A}{6\omega m} \frac{(kr_0)^4}{4+(kr_0)^4} \ . \qquad (Eq.10.2)$$

The damping ratio of an oscillating plate based on fluid dynamics theory is:

$$\xi''_{eq} = \frac{1}{4\pi^3} \frac{C_D A \rho_0 \Delta_0}{m} \ . \qquad (Eq.10.3)$$

The expression for the farfield amplitude of acoustic pressure of a baffled piston is:

$$p = \frac{P_0 R_0}{r} \sin(\omega t - kr) \ . \qquad (Eq.10.4)$$

Several experiments were designed to determine the applicability of these equations. The experimental methods and results are summarized in Table 10.1.

PROBLEM	TEST RESULTS	THEORY	
Pendulum	Tests	Oscillating Sphere	Fluid Dynamics
	2.22%	$6.2 \times 10^{-10}\%$	1%
	2.32%	$3.4 \times 10^{-9}\%$	1%
Unbaffled Plate	Tests	Oscillating Sphere	Fluid Dynamics
	0.02%	3.58%	0.0000532%
	0.03%	2.63%	0.000062%
Baffled Plate	Tests	Pulsating Sphere	
	N/A	0.34%	

Table 10.1: Damping Ratio Results

From Table 10.1, several observations are made:

1. The unbaffled plate experiment shows that neither acoustic theory nor fluid dynamics theory predicts damping ratio accurately at the given frequency of 5-10 Hz. We suspect that the unbaffled plate's vibrational frequency is too low for acoustic theory to be applied; on the other hand, it is too high for fluid dynamics theory to be applied. Therefore there may exist a frequency range in which neither acoustic theory nor fluid dynamics theory is applicable.
2. The pendulum experiment shows that fluid dynamics theory reasonably predicts the damping ratio of the system at low frequency vibration (around 0.2 Hz), but acoustic theory does not apply at this low frequency.
3. The baffled piston experiment shows acoustic theory (Rayleigh Integral) accurately predicts the farfield pressure of a clamped vibrating plate at a frequency of around 300 Hz. Acoustic theory works well for this

experiment. A theoretical damping ratio of the baffled plate is calculated, which seems to be reasonable. However within the scope of this project, it is too difficult to design an experiment to verify this result.

Thus it seems that fluid dynamics theory and acoustic theory work in two regimes when the frequency is very low and very high, respectively. Also there may exist a frequency range in which neither acoustic theory nor fluid dynamics theory is applicable individually. This naturally makes us wonder where the boundary between the two theories is. That is to say, can we find a dimensionless parameter that determines when to apply which theory?

10.2 Derivation of Dimensionless Parameter Γ for Vibrating Plate

The expression for the time-averaged acoustic power radiated from a pulsating sphere is derived in chapter 3, rewritten here:

$$\Pi_{ave} = 2\pi {r_0}^2 {u_0}^2 \rho_0 c_0 \frac{(kr_0)^2}{1+(kr_0)^2} \ . \qquad (Eq.10.5)$$

When $kr_0 \gg 1$, the vibrational frequency is high and the wave length is much smaller that the dimension of the sphere. The power radiated per unit surface area due to acoustic energy lost is:

$$W = \frac{\Pi_{ave}}{4\pi {r_0}^2}|_{kr_0 \gg 1} = \frac{1}{2} {u_0}^2 \rho_0 c_0 \ . \qquad (Eq.10.6)$$

This is the same expression as for radiation to one side from a rigid plate with a vibrational velocity amplitude, u_0. Now consider a vibrating plate with an infinite length, and a finite width, L. The vibrational amplitude is in the function of $\Delta = \Delta_0 \sin \omega t$, shown in Fig. 10.1(a).

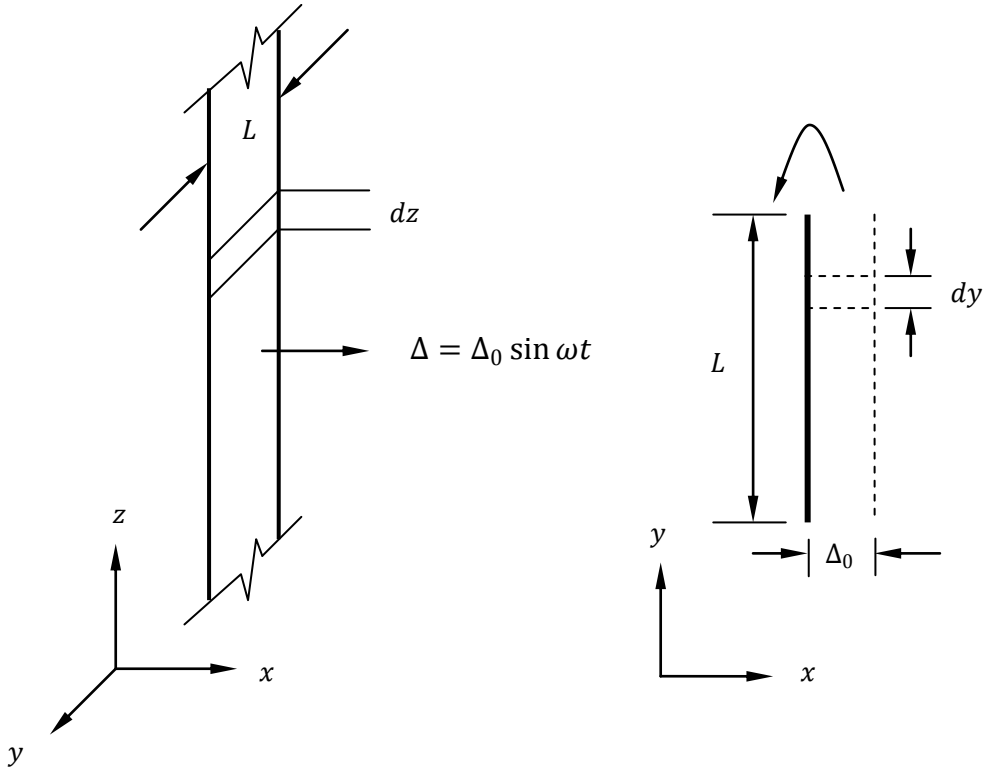

Fig. 10.1: A Vibrating Plate with Infinite Length, and Width L

Fig. 10.1(b) shows the cross section of the plate, looking in the negative z direction. When the plate is vibrating with an amplitude Δ_0, the air in the volume of $\Delta_0 L dz$ may flow back and forth from one side of the plate to the other. For each half cycle with a period of $T/2$, the infinitesimal air volume $\Delta_0 dydz$ moves a distance of $L/2$. Thus the average velocity of the air volume is:

$$v = \frac{L/2}{T/2} = \frac{L}{T} = \frac{\omega L}{2\pi} \ . \qquad (Eq. 10.7)$$

The kinetic energy of the infinitesimal air volume is:

$$E = \frac{1}{2}mv^2 = \int_{-\frac{L}{2}}^{\frac{L}{2}} \frac{1}{2}\rho_0 \Delta_0 dydz \left(\frac{\omega L}{2\pi}\right)^2 dy = \frac{\rho_0 \Delta_0 \omega^2 L^3}{8\pi^2} dz \ . \qquad (Eq. 10.8)$$

Assuming all the kinetic energy is dissipated (as heat) within each half cycle, the power lost to heat is then:

$$W_{flow} = \frac{E}{T} = \frac{\frac{\rho_0 \Delta_0 \omega^2 L^3}{8\pi^2} dz}{\frac{T}{2}} = \frac{\rho_0 \Delta_0 \omega^3 L^3}{8\pi^3} dz \ . \qquad (Eq. 10.9)$$

Since Eq. 10.6 is the power radiated per unit surface area, for the same infinitesimal air volume, the power radiated is:

$$W_{acoustic} = \frac{1}{2} {u_0}^2 \rho_0 c_0 (Ldz) \, . \qquad (Eq. 10.10)$$

Comparing Eq. 10.9 and Eq. 10.10, if $W_{flow} > W_{acoustic}$, which means the energy of acoustic radiation is less than the energy of fluid convection. In this case acoustic theory applies. Otherwise the energy dissipated due to air convection dominates and fluid dynamics theory applies. In mathematical form,

$$W_{flow} = \frac{\rho_0 \Delta_0 \omega^3 L^3}{8\pi^3} dz > \frac{1}{2} {u_0}^2 \rho_0 c_0 (Ldz) = W_{acoustic} \ . \qquad (Eq. 10.11)$$

In chapter 4, we have derived that the amplitude of velocity is given by:

$$u_0 = \Delta_0 \omega \ .$$

Substituting this relationship into Eq. 10.11 and simplifying, we obtain,

$$W_{flow} = \frac{\omega L^2}{4\pi^3} > \Delta_0 c_0 = W_{acoustic} \ , \qquad (Eq. 10.12)$$

or when

$$\Gamma = \frac{4\pi^3 \Delta_0 c_0}{\omega L^2} < 1 \ , \qquad (Eq. 10.13)$$

acoustic theory applies. In Eq. 10.13, Δ_0 is the amplitude of vibration, c_0 is sound speed, ω is the vibrational frequency and L is width of the plate. The proposed dimensionless parameter Γ approximately determines the limitation of applicability of acoustic theory and fluid dynamics theory.

10.3 Effect of Air upon Building Structures

In practice, most building structures' fundamental mode shapes can be thought

of as vibrating transversely. Thus the solutions for the damping ratio based on acoustic radiation from an oscillating sphere or fluid dynamics theory can be applied to calculate the damping ratio of a building structure. This idea is shown in Fig. 10.2.

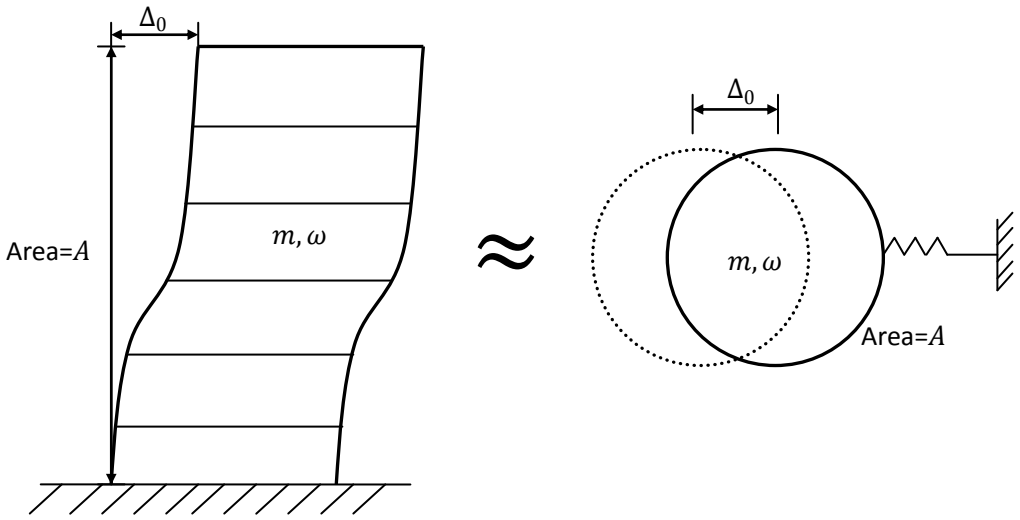

Fig. 10.2: General Multi-story Building Example

As shown in Fig. 10.2, a multi-story building structure can be approximated as a transversely oscillating sphere. Both of them have a vibrational amplitude, Δ_0; a projected area, A; a vibrational frequency, ω, and a mass, m.

If the building is vibrating transversely, the equivalent damping coefficient for this building can be calculated using Eq. 10.2 and Eq. 10.3, repeated here:

$$\xi_{oscillating} = \frac{\rho_0 c_0 A}{6\omega m} \frac{(kr_0)^4}{4 + (kr_0)^4} \ . \qquad (Eq. 10.14)$$

$$\xi_{fluid} = \frac{1}{4\pi^3} \frac{C_D A \rho_0 \Delta_0}{m} \ . \qquad (Eq. 10.15)$$

Which equation should be used depends on the dimensionless factor, Γ .

We are interested in how much air damping contributes to the total damping of a structure when different construction materials are used. Specific building examples are studied to find the equivalent damping ratios based on assumed building

properties. The examples assume the construction material is uniform reinforced concrete. The results are shown in table 10.2.

Building Type	A (m^2)	f (hertz)	m (ton)	Δ (m)	Γ	Theory	ξ (%)
1 story	50	15	2000	0.01	0.447	Acoustic	0.000098
5 stories	500	3	10000	0.05	5.587	FD	0.0000041
20 stories	5000	0.5	40000	0.2	53.636	FD	0.0000413
50 stories	25000	0.2	100000	0.5	167.61	FD	0.0002063

Table 10.2: Damping Ratios of Specific Steel Building Examples

Based on assumed building properties, different values of Γ are calculated to determine whether acoustic theory or fluid dynamics theory (indicated as FD in table 10.2) should be applied. The results show that for normal reinforced concrete buildings (usually with large mass values), the damping effect due to air is not significant.

The results can also be predicted by looking at Eq. 10.14 and Eq. 10.15. The major difference between applying these equations into practical buildings and into experiments is when studying the air damping effect upon buildings, the mass is usually large, leading to a small damping ratio; while the experimental devices we have developed are mostly light-weighted.

CHAPTER 11.

CONCLUSION

11.1 Summary and Significance

In previous chapters, detailed expressions for equivalent damping ratios based on acoustic radiation from a pulsating sphere and an oscillating sphere are presented. The equivalent damping ratio based on fluid dynamics theory is also presented. A solution to the farfield pressure amplitude of a baffled piston is derived. Experimental results and theoretical results have answered the questions we brought up in chapter 1.

(1) *Under what conditions does air affect the vibration of a building structure?*

Air enclosed in buildings introduces extra vibrational modes beyond to those have already existed when the building is in vacuum. The surrounding air has a small damping effect upon buildings.

(2) *How important is the effect of air on a vibrating building structure? Shall we consider air in analyzing buildings?*

Theoretical building examples shown in chapter 10 demonstrate that when designing buildings vibrating at low frequencies, the damping effect of air upon structures is not significantly considerable.

(3) *Under what conditions does a building structure's vibration cause sound and related acoustic impacts in air?*

A building structure's vibration causes acoustic radiation when the building's vibrational frequency is very high ($\Gamma < 1$, $kr_0 \gg 1$) and the wave length is much smaller than the building's dimensions.

(4) What type of physics should be used in determining structural damping?

Two types of physics are applied: acoustic theory and fluid dynamics theory. An unbaffled plate experiment and a pendulum experiment are designed to determine the applicability of the theoretical solutions to damping ratios. The results show that the solution to damping ratio based on acoustic works in high frequency vibrations only; the solution to damping ratio based on fluid dynamics theory works in the opposite low frequency vibrations. A baffled plate experiment is designed to test the Rayleigh Integral solution at relatively higher vibrational frequency. The theoretical solution matches well with the experimental results, verifying the applicability of acoustic theory in high frequency range. There might be a frequency range in which both acoustic theory and fluid dynamics theory should be applied simultaneously; it is also possible that neither these two theories are applicable in this frequency range. This range is a transition from the frequency range in which fluid dynamics theory applies only, to the frequency range in which acoustic theory applies only.

(5) When is acoustic theory appropriate, and when is fluid dynamics theory appropriate?

A dimensionless factor, Γ, is proposed to determine what physics should be applied in determining structural damping due to air. It determines whether acoustic theory or fluid dynamics theory should be applied based on vibrating structure's size, vibrational frequency, and vibrational amplitude. When $\Gamma > 1$ and the drag force are generated and fluid dynamics theory should be applied; when $\Gamma < 1$, acoustic theory should be applied. Further experiments are expected to verify this conclusion.

(6) Can we develop simple formulas that predict the damping effect of air on buildings?

The fluid dynamics theory can be applied directly to predict the damping effect of air on low-frequency vibration ($\Gamma > 1,\ kr_0 \ll 1$) buildings. For high-frequency vibration ($\Gamma < 1, kr_0 \gg 1$) buildings, acoustic theory should be applied to calculate the damping effect of air. We derived formulas to predict the damping effect of air on buildings.

11.2 Future Research

The conclusions of this thesis should be regarded as tentative until more experiments are conducted. Future possible experiments may include:

(1) Designing of high frequency vibration device for the purpose of determining the applicability of damping ratio based on acoustic theory experimentally.

(2) Designing devices including an unbaffled plate and a baffled plate vibrating at very high frequencies. It is favorable to have the frequency adjustable.

(3) Designing an oscillating rigid sphere whose vibrational frequency can be adjusted from very low to very high.

(4) Developing a theory which applies at the transition frequency range between fluid dynamics theory and acoustic theory ($\Gamma \cong 1$).

(5) More computational simulation including fluid-structure interaction and acoustic-structure interaction.

REFERENCES

ANSOL, Advanced Numerical Solutions: ansol.us/Products/Coustyx/Validation/MultiDomain/Radiation/Sphere/OscillatingSphere/Downloads/dataset_description.pdf

Anker, Jan Christian, 2005. "An Interpretation of the Physics of Fluid-Structure Interaction in the Frequency Domain", 23rd CADFEM User's Metting 2005, International Congress on FEM Technology with ANSYS CFX & ICEM CFD Conference. November, 2005. Germany.

Blackstock, David T., 2000. "Fundamentals of Physical Acoustics", 2000, John Wiley & Sons, Inc.

Chopra, Anil K. 2008. "Dynamics of Structures, Theory and Applications to Earthquake Engineering", 2008, 3rd Edition, Prentice-Hall Inc (Pearson Education Inc.).

Decultot, D., Lietard R., Chati F.. 2008. "Acoustic Radiation of Low Frequency Flexural Vibration Modes in a Submerged Plate", Acoustics'08 meeting, Paris, France, June 29- July 4, 2008.

Fahy, Frank; Gardonio Paolo, 2007. "Sound and Structural Vibration", 2nd Edition, Elsevier.

Gurgoze, M., 1999. "Receptance Matrices of Viscously Damped Systems Subject to Several Constraint Equations", Journal of Sound and Vibration, Volume 230, issue 5, pp 1185-1190.

Hasheminejad, Seyyed M., Azarpeyvand Mahdi, 2003. “Electricity Effects on Acoustic Radiation from a Spherical Source Suspended Within a Thermoviscous Fluid Sphere”, IEEE Transaction on Ultrasonics, Ferroelectrics, and Frequency Control. Volume 50, No.11, pp 1444-1454.

Hemmati, A.M. 2009. “Drag Measurement on an Oscillating Sphere in Helium II”, Journal of Low Temperature Physics 2009, Volume 156, pp 71-83.

Hong, K. L., Kim, J. 1995. “Analysis of Free Vibration of Structural-Acoustic Coupled Systems, Part I: Development and Verification of the Procedure”, Journal of Sound and Vibration, Volume 188, issue 4, pp 561-575.

Hong, K. L., Kim, J. 1996. “New Analysis Method for General Acoustic-Structural Coupled Systems”, Journal of Sound and Vibration, Volume 192, issue 2, pp 465-480.

Jacobson Mark F., Singh Rajendra, 1996. “Acoustic Radiation Efficiency Models of a Simple Gearbox”, NASA Technical Memorandum 107226. Seventh International Power Transmission and Gearing Conference.

Kozien, Marek S., Wiciak Jerzy, 2005. “Acoustic Radiation by set of L-joined Vibrating Plates”, Journal of Molecular and Quantum Acoustics, Volume 26 pp 183-190.

Lee, Y. 2006. “The Effect of Air on Structural Vibrations”. Master of Science in Civil Engineering Project, Department of Civil Engineering, University of New Mexico.

Mareddy, Shilpa. 2006. “An Analysis of Service Level Vibrations in A Utility Building”, Master of Science in Civil Engineering Project, Department of Civil Engineering, University of New Mexico.

Ngai K.W., Ng C.F., 2001. “Structure-Borne Noise and Vibration of Concrete Box Structure and Rail Viaduct”, Journal of Sound and Vibration, Volume 255, issue 2, pp 281-297.

Ortega, Rodriguez Carlos O., 2008. “Dynamic Gas-Solid Interaction”, Master of Science in Civil Engineering Thesis, Department of Civil Engineering, University of New Mexico.

Osaka, Yoshihiro, 2007. “Influence of Internal Damping on Vibration and Acoustic Radiation Characteristics of Rectangular Plate”, Proceedings of School of Engineering, Tokai University, Series E, July 2007.

Pierce, Allan D. 1989. “Acoustics, an Introduction to Its Physical Principles and Applications”, 1989 Edition, Acoustical Society of America.

Roberson, John A., Crowe Clayton T., 1975. “Engineering Fluid Mechanics”, 1975, Houghton Mifflin Company.

Ross, Mike R., 2004. “Coupling and Simulation of Acoustic Fluid-Structure Interaction System Using Localized Lagrange Multipliers”, 2004, Department of Aerospace Engineering Science, University of Colorado.

Oneline Sources:

Wikipedia, http://en.wikipedia.org/wiki/Density

Wikipedia, http://en.wikipedia.org/wiki/Wave_equation

Wikipedia, http://en.wikipedia.org/wiki/Barometric_formula

Wikipedia, http://en.wikipedia.org/wiki/Bulk_modulus

Wikipedia, http://en.wikipedia.org/wiki/Conservation_of_mass

Wikipedia, http://en.wikipedia.org/wiki/Material_derivative

Wikipedia, http://en.wikipedia.org/wiki/Wave

Wikipedia, http://en.wikipedia.org/wiki/Pendulum

Wikipedia, http://en.wikipedia.org/wiki/Phase_(waves)

Wikipedia, http://en.wikipedia.org/wiki/Interference_(wave_propagation)